Intermittent Fasting and Autophagy in MCF-7 Breast Cancer Cells: Towards Reprogramming the Tumor Microenvironment in Obese Patients

Final Degree Project

Biochemistry and Molecular Biology

Ariadna Subasic i López

Scientific director: Dr. Julio Madrigal Matute

Department of Preventive Medicine and Public Health

Universitat de València

Academic tutor: Dr. Iris Ginés Mir

Department of Biochemistry and Biotechnology

Universitat Rovira i Virgili

Universitat Rovira i Virgili

Tarragona, June 2025

To my family, for always believing in me, for shaping who I am, and for supporting me throughout my journey.

INDEX

Acknowledgements 6

Abbreviations 7

Abstract 8

1. **Introduction** 9

1.1. Breast Cancer (BC) Epidemiology and Public Health Relevance 9

1.2. Histological and Molecular Classification of BC 9

1.2.1. Molecular Classification 9

1.2.2. Histological Classification 10

1.3. Risk Factors 11

1.3.1. Non-Modifiable Risk Factors 11

1.3.2. Modifiable Risk Factors 11

1.4. ER+ Breast Tumors in Obese Patients: An Altered Tumor Microenvironment (TME) 12

1.4.1. Macrophage Plasticity and their Immunoregulatory Role in the TME .. 12

1.4.2. Macroautophagy (MA) and Chaperone-Mediated Autophagy (CMA): Mechanisms and Roles in Cancer 13

1.5. Intermittent Fasting (IF) as a Modulator of Autophagy and the TME 14

1.6. Knowledge Gap and Rationale for this Thesis 15

1.7. Hypothesis and objectives 16

2. **Materials and methods** 17

2.1. Cell Culture 17

2.2. Experimental Design: IF and Autophagy Modulation 17

2.3. Sample Collection 19

2.4. Cell Lysis and Sample Preparation 20

2.5. Protein Quantification by the Lowry Method 20

2.6. Solution Preparation and Western Blot Procedure 21

2.7. Quantification of Protein Expression by Western blot 25

2.8. Translational Perspective: Personalized Nutrition and Patient Care 25

3. **Results** 26

3.1. Cell Culture 26

3.2. IF in MCF-7 cells and Autophagy Modulation 26

3.2.1. Microscopic Analysis of MCF-7 Cells under Experimental Conditions 26

3.2.2. Protein Quantification by Lowry Assay 29
3.2.3. Protein Detection by Western Blot 31
3.2.4. Quantification of Protein Expression by Western Blot..... 31
3.3. Translational Perspective: Personalized Nutrition and Patient Care 38
4. **Discussion** 39
5. **Future Perspectives** 46
6. **Conclusion** 46
7. **Bibliography**..... 47
8. **Annexes**..... 50

Acknowledgements

This work was carried out within the Laboratory of Autophagy and Oncological Nutrition, part of the Department of Preventive Medicine and Public Health at the University of Valencia, under the supervision of Dr. Julio Madrigal Matute. I am deeply grateful to him for offering me the opportunity to participate in this emerging research line, for encouraging critical thinking, and for providing a collaborative and motivating working environment.

I am also grateful to the IBIONS team for welcoming me into such a dynamic environment and allowing me to take part in real consultations with breast cancer patients. Their work helped me understand the clinical value of personalized nutrition and inspired me through their professionalism and dedication. Participating in congresses and dissemination activities with them was a truly enriching experience.

I am thankful for Cecilia Sánchez Felipe, MSc student, for her support, daily companionship, and willingness to share ideas throughout this research period. Her presence made the work much more enjoyable and enriching.

I would also like to express my gratitude to my family, for their unconditional support, always.

I want to thank my friends: Jahaciel, Cinta, Paula, Marta and Judit for making these four years more special, I hope this is just the beginning of a lifelong friendship.

Finally, I would like to thank Dr. Iris Ginés Mir, my thesis supervisor, for her continuous support, insightful feedback, and kind guidance throughout this process. Her help has been essential to completing this project successfully.

VNIVERSITAT DE VALÈNCIA

ibions Instituto Biomédico Nutrición y Salud

Abbreviations

AMPK: AMP-activated Protein Kinase

ATG5: Autophagy Related Gene 5

BC: Breast Cancer

BSA: Bovine Serum Albumin

CMA: Chaperone-Mediated Autophagy

DMEM: Dulbecco's Modified Eagle Medium

ER: Estrogen Receptor

ER+: Estrogen Receptor-positive

FBS: Fetal Bovine Serum

GAPDH: Glyceraldehyde-3-Phosphate Dehydrogenase

HER2: Human Epidermal Growth Factor Receptor 2

HIF-1α: Hypoxia-Inducible Factor 1-alpha

HSC70: Chaperone Heat Shock Cognate Protein 70

IF: Intermittent Fasting

IVO: Instituto Valenciano de Oncología

LAMP2A: Lysosome-Associated Membrane Protein Type 2A

LC3: Microtubule-Associated Protein 1A/1B-Light Chain 3

MA: Macroautophagy

mTORC1: Mammalian Target of Rapamycin Complex 1

NL: Ammonium Chloride + Leupeptin (lysosomal inhibitors)

PBS: Phosphate Buffered Saline

PI3K/AKT: Phosphatidylinositol 3-Kinase / Protein Kinase B

PR: Progesterone Receptor

SD: Standard Deviation

SDS-PAGE: Sodium Dodecyl Sulphate Polyacrylamide Gel Electrophoresis

SQSTM1/P62: Sequestosome-1 / P62

STAT3: Signal Transducer and Activator of Transcription 3

TAMs: Tumor-Associated Macrophages

TBST: Tris-Buffered Saline with Tween 20

TME: Tumor Microenvironment

TNBC: Triple-Negative Breast Cancer

VEGF: Vascular Endothelial Growth Factor

WB: Western Blot

Abstract

Breast cancer (BC) is the most prevalent cancer among women worldwide, with estrogen receptor-positive (ER+) subtypes constituting most cases. In the context of obesity, ER+ tumors often develop an immunosuppressive tumor microenvironment (TME), characterized by chronic inflammation, pathological angiogenesis, and altered macrophage plasticity. Autophagy, particularly macroautophagy (MA) and chaperone-mediated autophagy (CMA), plays a critical role in maintaining cellular homeostasis and modulating immune responses. Intermittent fasting (IF) has emerged as a promising strategy to activate autophagy and reprogram the TME; however, it remains unclear how many fasting cycles are needed to induce significant autophagic responses.

This study aimed to compare the activation of MA and CMA in MCF-7 cells subjected to one, two, or three fasting cycles. Two time-dependent fasting protocols were implemented: a 4-hour fasting model to assess MA and a 16-hour model to evaluate CMA. To evaluate autophagic responses, Western blot analysis was performed on LC3, SQSTM1/p62, and GAPDH with and without lysosomal inhibitors to assess autophagic flux, while the expression levels of ATG5 and LAMP2A were analysed independently as markers of the autophagic machinery.

Repeated fasting cycles appeared to progressively enhance autophagy activation, particularly for MA markers such as LC3 and SQSTM1/P62, whereas CMA markers showed more variable patterns. Despite the limited sample size (n=2), the findings suggested that three fasting cycles may be more effective than a single cycle in inducing autophagic responses.

These preliminary results support the potential of IF as a complementary strategy to modulate the TME in obesity-associated ER+ BC. Further studies with increased replicates and functional validation are necessary to confirm these observations.

Key Words: Breast cancer, Estrogen receptor-positive (ER+), obesity, Tumor microenvironment (TME), Intermittent fasting, Macroautophagy (MA), Chaperone-mediated autophagy (CMA), MCF-7 cells, LAMP2A.

1. Introduction

1.1. Breast Cancer (BC) Epidemiology and Public Health Relevance

Breast cancer (BC) is the most diagnosed malignancy among women and the most prevalent cancer globally (1). In 2020 BC accounted for 2,3 million new cases and approximately 685.000 deaths worldwide, representing 11,7% of all new cancer cases and 6,9% of all cancer deaths (1). In Spain, BC remains the most frequently diagnosed tumor in women, with an estimated 35.000 new cases each year and 6.606 deaths in 2020 (1). Although mortality has declined in recent decades, thanks to improved screening, earlier diagnosis, and advances in treatment, the incidence continues to grow, partially due to risk factors such as delayed childbearing, reduced breastfeeding, sedentary behavior, obesity, and alcohol consumption (2, 3).

Despite advances in early detection and treatment, survival for metastatic BC remains poor, with five-year survival rates below 30% (3). These numbers show the enormous impact of BC on global health systems (4). Given these trends, more research into BC biomarkers and improving therapies is essential to improve the mortality rates, nevertheless, we should not overlook the importance of cancer prevention efforts in reducing incidence.

1.2. Histological and Molecular Classification of BC

1.2.1. Molecular Classification

BC is a heterogeneous disease having multiple subtypes defined by different molecular markers, gene expression patterns, and clinical characteristics (5). The main subtypes are luminal estrogen receptor (ER)-positive (luminal A and luminal B), human epidermal growth factor receptor 2 (HER2)-positive and triple-negative breast cancer (TNBC) (5, 6), classified based on the presence or absence of hormone receptors such as estrogen, progesterone, and human epidermal growth factor (HER) (5), as summarized in **Table 1**.

Around 65–70% of BCs are ER+ or PR+ and respond to endocrine therapies like tamoxifen (6), which inhibit ER signalling (7). Although PR binds progesterone, its expression depends on ER activity, meaning ER inhibitors can also be effective in PR+ tumors (8, 9).

Approximately 20% of BC overexpress HER2 (8), associated with a more aggressive disease course and poorer prognosis (6). Overactivation of HER2 triggers oncogenic

signalling pathways, leading to rapid tumor growth (5). These are typically treated with targeted therapies that block HER2 signalling, such as Herceptin (10). Lastly, TNBC, which lack ER, PR, and HER2, account for about 15% of cases (8) and are unresponsive to hormone or HER2-targeted therapies, chemotherapy with anthracyclines and taxanes remains the standard (11),although newer therapies like immune checkpoint inhibitors (e.g., atezolizumab (12) or pembrolizumab (13)) and PARP inhibitors (e.g., Olaparib (14)) have been approved for specific subtypes of TNBC.

Additionally, Ki67 protein serves as a marker of cell proliferation (6). High Ki67 levels are linked to more aggressive tumors and poorer outcomes, as the Ki67 index indicates how quickly the cancer cells are dividing (5, 15).

Table 1. *Characteristics of molecular subtypes of BC.*

	Luminal A	**Luminal B**	**HER2**	**TNBC**
Frequency (%)	50	15	20	15
ER	+	+	+/-	-
PR	+	+/-	+/-	-
HER	-	-	+	-
Ki67%	Low (<14%)	High (>14%)	High (>14%)	High (>14%)
Therapy used	Hormonal	Hormonal/Chemo	Hormonal/Chemo/Herceptin	Chemo/Experimental

ER: estrogen receptor; PR: progesterone receptor; HER: human epidermal growth factor; TNBC: triple negative breast cancer. Adapted from Orrantia-Borunda, E. *et al*. (2022) (5).

However, the cancer's stage at diagnosis also influences prognosis and treatment options. Therefore, a comprehensive assessment of the cancer subtype, stage, and other clinical factors is necessary to determine each patient's most appropriate treatment strategy (16).

1.2.2. Histological Classification

BC cancer tumors can be distinguished by their anatomical origin (8). Specifically, they are categorized as either ductal carcinomas, which develop in the milk ducts, or lobular carcinomas, which originate in the breast lobules (15). Furthermore, both ductal and lobular carcinomas can be classified as invasive, if cancer cells have spread into surrounding breast tissue, or non-invasive (*in situ*), when the tumor remains confined to its original location (15).

1.3. Risk Factors

1.3.1. Non-Modifiable Risk Factors

There is a large variety of risk factors associated with BC, including both modifiable and non-modifiable risk factors.

Among the non-modifiable risk factors for BC, female sex and increasing age are key contributors due to hormonal exposure and accumulation of genetic damage and environmental carcinogens (17). A positive family history, especially first-degree relatives affected by BC, significantly raises risk, as do germline mutations in *BRCA1*, and *BRCA2,* which encode proteins essential for the repair of DNA double-strand breaks through homologous recombination, contributing to genomic stability (17). Other important risk factors include high mammographic breast density and ethnicity, with white, non-Hispanic women showing the highest incidence and black women experiencing higher mortality, likely influenced by differences in healthcare access and socioeconomic conditions (17).

1.3.2. Modifiable Risk Factors

Several modifiable factors significantly influence BC risk. These include certain pharmacological agents (such as diethylstilbestrol, due to its strong estrogenic activity, during pregnancy and long-term hormone replacement therapy), physical inactivity, high body mass index, alcohol consumption, tobacco use, and poor dietary habits, among others (17). Prolonged use of antidepressants, extended antibiotic treatments, and tetracycline may be linked to increased risk, though mechanisms remain unclear (17). Tobacco, whether active or passive, exposes breast tissue to carcinogens such as those affecting *TP53,* which encodes the tumor suppressor protein p53, which regulates the cell cycle and promotes DNA repair or apoptosis. Alcohol contributes by raising estrogen levels and causing oxidative DNA damage (17). Additionally, diets rich in processed foods, refined sugars and saturated fats, together with being overweight or obesity, promote inflammation and hormonal imbalances that create a tumor-promoting environment (17).

In contrast, regular physical activity has a protective effect against BC, due to its beneficial influence on weight regulation, hormone balance, immune function and systemic inflammation (17).

1.4. ER+ Breast Tumors in Obese Patients: An Altered Tumor Microenvironment (TME)

ER+ BC is the most prevalent subtype, often associated with lower immunogenicity and better prognosis compared to TNBC or HER2+ subtypes. However, many ER+ tumors fail to respond to immunotherapies (especially inhibitors of the PD-1/PD-L1 axis) or antiangiogenic treatments, because they are considered immunologically "cold" tumors, characterised by low mutational load, poor lymphocyte infiltration, and limited antigen presentation, leading to inadequate T cell activation and resistance to immune checkpoint inhibitors (18).

In obesity, this "cold" phenotype is worsened by changes in the tumor microenvironment (TME). Obesity induces chronic low-grade inflammation and systemic metabolic dysfunction, which promote the release of pro-inflammatory cytokines, adipokines and growth factors (19). These factors activate oncogenic pathways such as nuclear factor kappa-light-chain-enhancer of activated B cells (NF-κB), phosphatidylinositol 3/protein kinase B (PI3K/AKT) and signal transducer and activator of transcription 3 (STAT3), which drive tumor cell proliferation, immune evasion, and pathological angiogenesis (20). One of the main features of the obese TME is the induction of hypoxia due to excessive tissue expansion and abnormal vascular architecture, which stabilizes hypoxia-inducible factor 1-alpha (HIF-1α) and upregulates vascular endothelial growth factor (VEGF) expression, promoting the formation of structurally immature and leaky blood vessels (21). These vessels not only facilitate metastasis but also impair drug delivery and contribute to therapy resistance. Collectively, these factors create a more aggressive and therapy-resistant tumor profile in obese ER+ patients (22).

1.4.1. Macrophage Plasticity and their Immunoregulatory Role in the TME

Macrophages are the most abundant immune cells in the breast TME, especially in ER+. These tumor-associated macrophages (TAMs) can adopt different phenotypes: M1-like (pro-inflammatory and antitumor) or M2-like (immunosuppressive and pro-tumorigenic), depending on local metabolic and cytokine signals (23). In obesity-associated ER+ BC, TAMs shift more to M2-like phenotype, promoting tumor progression through VEGF secretion, immunosuppression and extracellular matrix remodelling (24). This polarization is driven by signals inside the tumoral environment, but the mechanisms that regulate this phenotypic plasticity are not completely characterised, especially in antitumoral immunity and in "cold tumors" like ER+ BC (23).

This polarization is influenced by the metabolic environment, where M1 macrophages rely on glycolysis and M2 on oxidative phosphorylation and fatty acid oxidation (24). Autophagy, particularly chaperone-mediated autophagy (CMA), has emerged as a regulator of this process, with CMA targeting pro-angiogenic proteins like intercellular adhesion molecule 1 (ICAM-1) (25). Therefore, targeting macrophage plasticity through metabolic and autophagic modulation represents a promising strategy to reprogram the TME towards an immunostimulatory state, particularly beneficial in ER+ tumors associated with obesity.

1.4.2. Macroautophagy (MA) and Chaperone-Mediated Autophagy (CMA): Mechanisms and Roles in Cancer

Autophagy is a lysosome-dependent process essential for maintaining cellular homeostasis by degrading damaged organelles and misfolded proteins (26). The two main types relevant in cancer are macroautophagy (MA) and CMA (27) (**Figure 1**). MA involves the formation of autophagosomes that engulfs cytoplasmic material (28) and fuses with lysosomes, allowing the degradation of its proteins by lysosomal hydrolases. This process is regulated by autophagy-related (ATG) proteins such as ATG5, which participates in the early steps of autophagosome formation through its conjugation with ATG12 and association with ATG16. Additionally, microtubule-associated protein 1A/1B-light chain 3 (LC3), particularly its lipidated form LC3-II, is incorporated into the autophagosomal membrane, and plays a crucial role in adapting to metabolic stress, including nutrient deprivation and hypoxia (28). Another important component is sequestosome-1/P62 (SQSTM1/P62), a selective autophagy adaptor that binds ubiquitinated cargo and LC3-II, targeting them for degradation. CMA, by contrast, is a highly selective pathway where soluble proteins containing a KFERQ-like motif are recognized by the cytosolic chaperone heat shock cognate protein 70 (HSC70) and transported inside the lysosome (28) via lysosome-associated membrane protein type 2A (LAMP2A), the rate-limiting receptor for CMA, where they will be degraded. For example, glyceraldehyde-3-phosphate dehydrogenase (GAPDH), a glycolytic enzyme, contains KFERQ-like motif and is a well-characterised substrate of CMA. Unlike MA, CMA acts on individual proteins and does not require vesicle formation, allowing control of proteostasis (28). During prolonged fasting, CMA becomes more active as MA declines, supporting selective protein degradation (29).

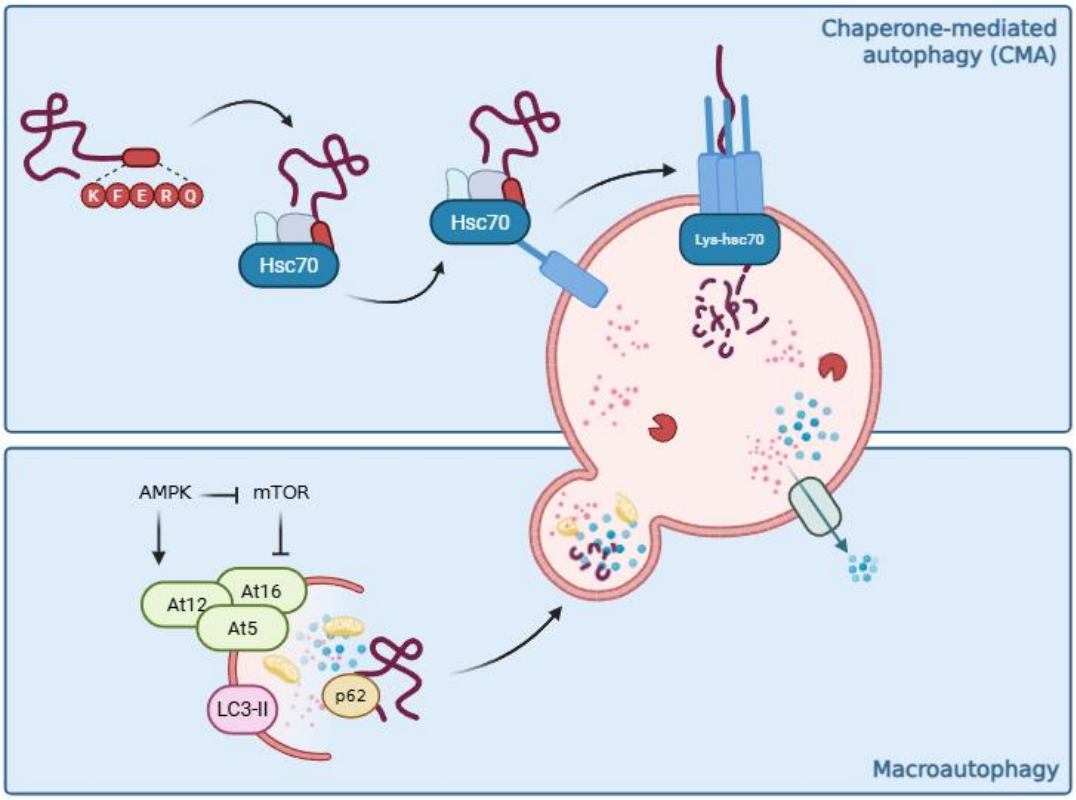

Figure 1. *Molecular mechanism of chaperone-mediated autophagy and macroautophagy. Self-creation by Biorender.*

In cancer, autophagy has dual roles depending on the context. In early tumorigenesis, it acts as a tumor suppressor by limiting oxidative stress and genomic stability (27). However, in advanced tumors it is often supports cancer cell survival under metabolic and therapeutic stress (27). CMA is frequently upregulated in cancer, promoting metabolic reprogramming, resistance to apoptosis and drug resistance (29). High levels of LAMP2A have been observed in breast tumors, including ER+ subtypes, and are linked to poor prognosis and reduced treatment response (29). In obesity, chronic metabolic stress may dysregulate CMA in TME, and restoring its balance could improve immune management and reduce inflammation and angiogenesis (30).

1.5. Intermittent Fasting (IF) as a Modulator of Autophagy and the TME

Intermittent fasting (IF) is emerging as a promising non-pharmacological strategy to modulate tumor metabolism, improving treatment response and reducing adverse effects (31), partly through activation of autophagy (27). Fasting lowers levels of insulin, insulin-like growth factor 1 (IGF-1) and leptin, hormones elevated in obesity and associated with tumor progression and treatment resistance (32), while activating nutrient-sensing

pathways such as 5' AMP-activated protein kinase (AMPK) and inhibiting mammalian target of rapamycin complex 1 (mTORC1), a key suppressor of autophagy (33).

Autophagic responses to fasting are time- and context-dependent. MA is rapidly induced during the early hours of fasting (34), while CMA requires prolonged or repeated fasting due to its selective mechanism and need for LAMP2A upregulation (34)(35). In obesity-associated ER+ BC, where CMA is often impaired, IF may help restore its function (36), promoting degradation of oncogenic proteins, reducing metabolic stress and shifting TAMs from pro-tumor M2-like to an antitumor M1-like phenotype (37-39).

Overall, IF could reprogram both tumor and immune cells in the TME, helping to counteract obesity-driven immunosuppression and improve therapeutic outcomes in ER+ BC.

1.6. Knowledge Gap and Rationale for this Thesis

Despite the growing interest in the role of autophagy in cancer, and the increasing evidence linking nutritional interventions to improved therapeutic outcomes, a critical knowledge gap remains: how many cycles of intermittent fasting are necessary to induce meaningful and sustained activation of MA and CMA in ER+ BC cells.

While MA is known to respond quickly to nutrient deprivation, CMA exhibits a delayed and cumulative activation pattern, often requiring repeated or extended fasting to reach full functionality (34). Preliminary studies suggest that repeated cycles of fasting might have better outcomes (40). However, the mechanisms behind remain unknown. So, **direct experimental comparisons between different numbers of fasting cycles and autophagy activation** remain lacking.

This knowledge gap is relevant in ER+ BC associated with obesity, where CMA is both upregulated in tumor cells and functionally impaired in immune cells. Chronic metabolic overload, lysosomal saturation, and sustained inflammation may disrupt normal CMA flux, limiting its capacity to degrade oncogenic proteins and modulate immune responses. If IF can **restore or enhance CMA activity**, it may offer a means to reprogram the TME, shifting macrophage polarization toward antitumor phenotypes, reducing pathological angiogenesis, and enhancing overall immunocompetence.

Understanding whether a higher number of fasting cycles leads to superior activation of CMA and MA could inform the design of personalized dietary interventions as

coadjuvant strategies for BC patients with obesity, aiming to improve response to standard therapies and reduce recurrence.

1.7. Hypothesis and objectives

Hypothesis

Repeated cycles of IF progressively activate MA and, more notably, CMA in ER+ BC cells. Consequently, three fasting cycles will achieve more robust CMA and MA activation. This enhanced autophagic response may counteract the metabolic and immune dysfunctions characteristic of the obese, potentially improving therapeutic outcomes when used as a coadjuvant strategy.

General Objective

To evaluate whether one, two, or three cycles of IF differentially activate MA and CMA in MCF-7 BC cells, and to determine whether this modulation could support the development of coadjuvant dietary strategies for reprogramming the TME in ER+ BC associated with obesity.

Specific Objectives

1. **To investigate differential activation of CMA and MA under fasting conditions**, taking into consideration different induction times.
2. **To compare the activation of MA and CMA after one, two, or three fasting cycles** by quantifying the expression of key autophagy markers: LC3-II, ATG5, SQSTM1/P62, LAMP2A and GAPDH.
3. **To analyse the accumulation of autophagy substrates in the presence and absence of lysosomal inhibitors** to assess whether autophagic flux is progressively enhanced with increasing fasting cycles.
4. **To contribute experimental evidence to support the use of IF as a therapeutic tool** for reprogramming proteostasis and immune dynamics in the context of obesity-driven ER+ BC.
5. **To highlight the role of personalized nutrition as a translational application of cancer research**, emphasizing the need to communicate scientific findings to patients and healthcare professionals as part of an integrative oncology approach.

2. Materials and methods

2.1. Cell Culture

The study used MCF-7 cells; a luminal A subtype ER+ breast adenocarcinoma cell line derived from a pleural effusion of a 69-year-old female patient (41). These cells are adherent cells that grow as monolayers and form cell aggregates, which are well-characterized for their epithelial-like morphology, hormone receptor expression (ER-α, progesterone, androgen), and relevance to breast cancer biology (41).

Cells were maintained in high-glucose Dulbecco's Modified Eagle Medium (DMEM) (DMEM-HPSTA, Capricorn scientific, Germany), supplemented with 10% fetal bovine serum (FBS) (FBS-11A, Capricorn Scientific, Germany) and 1% penicillin/streptomycin (P/S) (L0018-100, Biowest, USA) and renewed medium 2 to 3 times per week. MCF-7 were grown in a humidified incubator at 37°C with 5% CO_2.

2.2. Experimental Design: IF and Autophagy Modulation

MA is known to be activated early during nutrient deprivation, with a peak response typically observed around 4 hours of fasting (34). On the other hand, CMA activation happens later, becoming more active after approximately 16 hours of fasting (34).

To capture these time-dependent effects, MCF-7 cells were seeded at a density of 350.000 cells/mL to ensure optimal confluency in a 6-well plate. Before seeding, adherent cells were washed with 2 mL of phosphate buffered saline (PBS) (21-040-CVR, Corning, USA) twice, then 2 mL of trypsin (25200056, Thermo Fisher Scientific, USA) were added in order to lift the cells (time: looking at the microscope, until all cells were lifted). Then 2 mL of the supplemented high-glucose DMEM were added to stop the trypsin reaction. Cells were then centrifuged (300xg, 5 min, 18ºC) to separate the cells from the supernatant. Finaly, they were resuspended in fresh culture medium and plated in 6-well plates at a final density of 350.000 cells/mL.

Two fasting protocols were used in parallel (**Figure 2**), using FBS-free DMEM: a 16-hour fasting period for CMA induction and a 4-hour fasting period for MA induction. The experimental conditions included a control (complete medium with 10% FBS and 1% P/S), and three fasting conditions (A1, A2, A3), where the number means the number of fasting cycles completed.

Additionally, in the final cycle, subsets of each condition were treated with leupeptin hemisulphate (J61188.MC, Thermo Fisher Scientific, USA) 10 mM, and NH_4Cl (123340010, Thermo Fisher Scientific, USA) 150 mM. These inhibitors (NL) impair lysosomal degradation by neutralizing acidic pH (NH_4Cl) and blocking protease activity (leupeptin), allowing the accumulation of undegraded substrates (42, 43) and help to asses autophagic flux (44). Each condition was performed in quadruplicate (n = 4) to ensure statistical robustness. This enables the distinction between enhanced autophagy induction and reduced degradation. Eight conditions were assessed for each protocol: control, control + inhibitors, and one to three fasting cycles, with or without inhibitors.

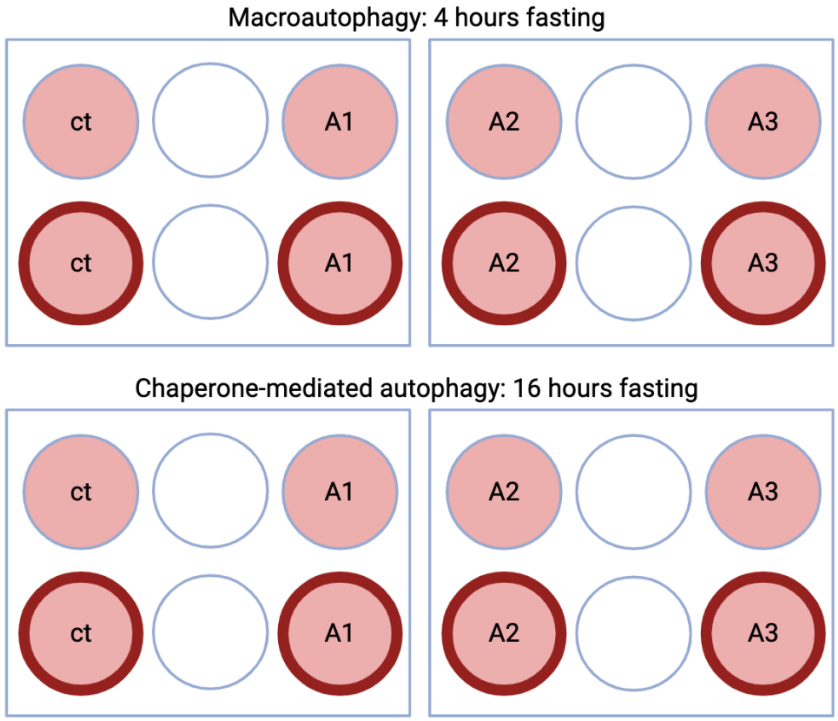

***Figure 2**. Plate design. Control: 24 hours complete growth medium; A1: 1 fasting cycle; A2: 2 fasting cycles; A3: 3 fasting cycles. Red circle: in the last cycle, NH4CL 10 mM and leupeptin 150 mM were added.*

To evaluate the activation of CMA and MA under fasting conditions, a synchronized experimental schedule was implemented. In all replicates the same cells were seeded on Friday at a final concentration of 350,000 cells/mL in 6-well plates and maintained in complete growth medium (DMEM supplemented with 10% FBS and 1% penicillin-streptomycin) until the initiation of the fasting cycles.

On the following Tuesday at 16:00, the first fasting cycle for CMA condition A3 was initiated. Before medium replacement, cells were washed twice with 1,2 mL of pre-warmed 1× PBS to remove serum residues. FBS-free DMEM (fasting medium) was then

added. After 16 hours of fasting, at 8:00 on Wednesday, the fasting medium was replaced with complete growth medium in all CMA wells to have same conditions in all the wells.

Simultaneously, the first 4-hour fasting cycle for MA condition A3 was started, following the same PBS washing and fasting medium replacement steps as mentioned before. At 12:00, fasting ended, and complete growth medium was renewed to all MA wells.

At 16:00 on Wednesday, the second CMA fasting cycle for A3 and the first for A2 were initiated. The next morning (Thursday at 8:00), fasting media was replaced with complete growth medium in all CMA wells. In parallel, the second MA fasting cycle for A3 and the first for A2 began at 8:00 and concluded at 12:00 of Wednesday, when complete medium was added back to all MA wells.

The third and final fasting cycle for conditions A1, A2, and A3 (CMA) was started on Thursday at 16:00. At this time, fasting medium with autophagy inhibitors was freshly prepared. Experimental groups included:

- Control (complete growth medium).
- Control + lysosomal inhibitors, NH_4Cl and leupeptin (NL) (complete growth medium with 10 mM NH_4Cl and 150 µM leupeptin).
- A1, A2, and A3 fasting (serum-free DMEM).
- A1, A2, and A3 fasting + lysosomal inhibitors (serum-free DMEM supplemented with 10 mM NH_4Cl and 150 µM leupeptin).

The CMA experiment ended on Friday at 8:00, after all fasting cycles had been completed. At this point, the final 4-hour fasting cycle for MA A1, A2, and A3 was initiated using the same procedure as described for CMA. The MA experiment was finished at 12:00 on Friday.

2.3. Sample Collection

Following the final fasting cycles for both CMA and MA conditions, all samples were collected using the same protocol, samples were handled all the time on ice to preserve protein integrity.

First, the fasting medium was removed from each well. Wells were then washed with 2 mL of cold PBS to eliminate residual medium. Cells were then collected by scraping: initially with 800 µL of cold PBS, followed by a second scraping with 200 µL to make

sure there is the minimum of cell loss. The total 1 mL of PBS containing the cells was transferred into 1,5 mL microcentrifuge tubes and centrifuged at 2000×g for 5 minutes at 4 °C. After centrifugation, the supernatant was discarded, and the cell pellet was resuspended in 50 µL of lysis buffer. Samples were then stored at −80 °C until further analysis (cell lysis).

The lysis buffer with protease inhibitors (PI) was made of 0,25 M sucrose with a protease inhibitor mix. Preparation steps were as follows, in a 50 mL tube, the following inhibitors were added: Leupeptin hemisulphate (50 mg), AEBSF Clorhidrato BioChemica (A1421,0500, ITW Reagents, Germany), USA) (50 mg), 4 mL of water and vortex. Pepstatin A (P4265, Sigma-Aldrich, USA) was prepared separately due to its methanol solubility, dissolved in 100% methanol (10626652, Thermo Fisher Scientific, USA) to a final concentration of 6.8 mg/mL (e.g., for 1.36 mg, add 200 µL methanol), then add 200 µL of this Pepstatin A solution to the main mix, 4 mL of 0.5 M EDTA (EDTA-00A-1K0, Labbox, Spain) (pH 7.5–8.0) to the inhibitor solution. Finally, vortex and adjust the final volume to 20 mL with PBS. Aliquots of the final lysis buffer of 1 mL were made and stored at −20 °C.

2.4. Cell Lysis and Sample Preparation

Frozen cell pellets with lysis buffer stored at −20 °C were transferred on ice to maintain protein integrity. All following steps were done on ice to minimize proteolysis and preserve post-translational modifications. Cell lysis was performed by sonication using the Sonicator model FB120 Fisherbrand (FB120, Fisher Scientific, USA), applying a 10-second pulse at 20% amplitude. In this step, plasma membrane is disrupted but needs to be done carefully to not overheat the sample and prevent protein denaturalization. The resulting mix, containing total soluble proteins, was collected and used for protein quantification measurements using the Lowry method. After the Lowry, samples were stored at -20ºC for following analysis.

2.5. Protein Quantification by the Lowry Method

Total protein concentration was determined using the Lowry method, a colorimetric assay based on the reaction between peptide bonds and copper ions under alkaline conditions, followed by reduction of the Folin-Ciocalteu reagent, resulting in a measurable color change proportional to protein content (45).

The assay was performed in a 96-well plate, with technical duplicates for each sample to ensure reliability. A standard curve was generated using bovine serum albumin (BSA) (A1391,0050, ITW Reagents, Germany) at final volumes of 0, 2, 5, 7, 10, 15, and 20 µL of a 1 mg/mL stock solution (stored at 4 °C), with water added to reach 25 µL in all wells. For experimental samples, 2 µL of lysate were added to 23 µL of distilled water.

The Lowry solutions were prepared as follows: Solution A (40 g/L Na_2CO_3 (SOCA-00P-500, Labbox, Spain) and 4 g/L NaOH (SOHY-P0A-500, Labbox, Spain)) and Solution B (0.5% $CuSO_4$ (CUSU-A0A-250, Labbox, Spain) and 1% sodium citrate (10396430, Thermo Fisher Scientific, USA)) were both kept at room temperature and mixed freshly before use at a 50:1 A:B ratio. To each well, 150 µL of the A:B mixture was added, followed by 15 µL of Folin-Ciocalteu reagent (251567.1609, ITW Reagents, Germany) (1 M, room temperature), added quickly due to its photosensitive nature. The plate was incubated for 20 minutes at 37 °C in the dark to allow color development.

Absorbance was then measured at 675 nm using the spectrophotometer SpectraMax Plus 384 Microplate Reader, and protein concentrations were calculated based on the standard curve generated from BSA samples.

2.6. Solution Preparation and Western Blot Procedure

For electrophoresis and protein transfer, various buffer solutions were prepared. A 1,5 M Tris buffer (pH 8,8), used to prepare the resolving gel, and a 0,5 M Tris-HCl buffer (pH 6,8), used to prepare the stacking gel, were prepared using standard protocols, providing the appropriate pH conditions for protein separation. The 10X electrophoresis running buffer contained 30,3 g of Tris base (15538844, Thermo Fisher scientific, USA), 144 g of glycine (131340.1211, ITW reagents, Germany), and 10 g of SDS (142363.1211, ITW reagents, Germany), adjusted to pH 8.3 and brought to a final volume of 1 L with distilled water. Prior to use, it was diluted 1:10 to obtain a 1X working solution. The transfer buffer consisted of 25 mM Tris base, 190 mM glycine, 20% methanol, and 0,1% SDS, pH adjusted to 8,3. The 4X loading buffer was composed of 4 mL of 100% glycerol (158920010, Thermo Fisher Scientific, USA), 4,8 mL of Tris-HCl (pH 6,8), 0,8 g of SDS, 4 mg of bromophenol blue (BRPH-B0D-005, Labbox, Spain), 0,5 mL of β-mercaptoethanol (125472500, Thermo Fisher Scientific, USA), and 0,7 mL of distilled water. The Ponceau S (J60744.09, Thermo Fisher Scientific) staining solution, used to temporarily stain proteins on a membrane after transfer in Western blotting, allows the

verification of successful and uniform protein transfer before antibody incubation, was prepared by dissolving 0,033 g of the dye in 10 mL of 0,1% acetic acid 100% (27225, Riedel-de Haen, Germany), adjusted to a final volume of 30 mL with distilled water.

Sodium dodecyl-sulfate polyacrylamide gel electrophoresis (SDS-PAGE) gels were cast with a 12% separating gel, for bigger proteins, and 15% separating gel for smaller proteins, and a stacking gel. For two gels, the 12% resolving gel solution contained 6,6 mL of distilled water, 8 mL of 30% acrylamide (A3626,1000, ITW Reagents, Germany), 5 mL of 1,5 M Tris (pH 8,8), 0,2 mL of 10% SDS (142363.1211, ITW Reagents, Germany), 0,2 mL of 10% ammonium persulfate (APS) (131138.1211, ITW Reagents, Germany), and 8 µL of Tetramethylethylenediamine (TEMED) (10689543, Thermo Fisher Scientific, Germany). Two gels of 15% contained 4,6 mL of distilled water, 10 mL of 30% acrylamide, 5 mL of 1,5 M Tris (pH 8,8), 0,2 mL SDS 10%, 0,2 mL APS 10% and 0,008 mL of TMED. The stacking gel solution was composed of 5.5 mL of distilled water, 1.3 mL of 30% acrylamide solution, 1 mL of 0.5 M Tris (pH 6,8), 0,08 mL of 10% SDS, 0,08 mL of 10% APS, and 8 µL of TEMED. Before starting, the glass plates were cleaned with 70% ethanol. After pouring the resolving gel, 1 mL of methanol was added to prevent air bubbles during polymerization. After 20 minutes, the methanol was removed, the stacking gel was poured, and polymerization happened for an additional 20 minutes. The gels were then stored in distilled water and sealed with a moist paper at 4 °C overnight.

The following day, protein samples were loaded into the gel wells using 1X running buffer. Molecular weight ladder (26619, Thermo Fisher Scientific, USA) (5 µL) was loaded in the first well. Each sample was prepared to contain 20 µg of total protein in 16 µL of total volume, mixed with 4 µL of 4X loading buffer to obtain a final 1X dilution. An example of sample layout, corresponding to the experiment of 3 fasting cycles, is shown in **Figure 3**. Electrophoresis was running at 100 V for 20 minutes to allow sample stacking, followed by 150 V until the dye front was near the bottom of the gel (near 1 hour total).

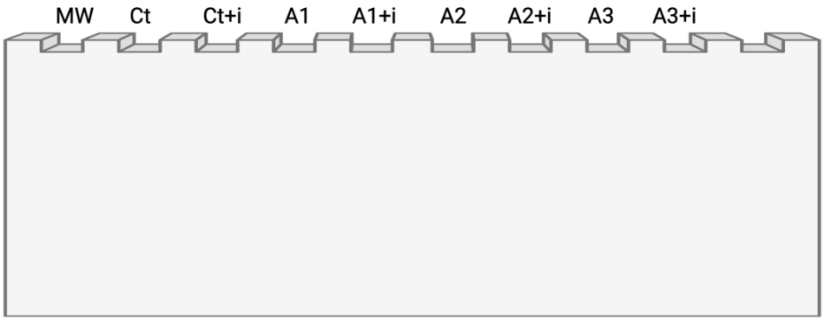

***Figure 3**. Sample layout for electrophoresis.*

Proteins were transferred onto nitrocellulose membranes using a wet transfer system. The gel and membrane were assembled in a "sandwich" manner with sponges and filter papers, and transfer was performed at 100 V for 60 minutes in cold transfer buffer (1X) and with ice. Protein transfer was confirmed by staining the membrane with Ponceau S.

10X Tris-buffered saline with 0,1% Tween 20 detergent (TBST) buffer was prepared with 24 g of Tris base, 88 g of NaCl (11984051, Thermo Fisher Scientific, USA), and 24 mL of Tween-20 (10485733, Thermo Fisher Scientific), adjusted to pH 7,6 and brought to a final volume of 1 L. Membranes were blocked in 5% skimmed powder milk diluted in TBST 1X and 0,02% sodium azide (190381000, Thermo Fisher Scientific, USA) for an hour. The primary antibody incubation was performed overnight at 4 °C. Anti_LC3B (Cell Signaling 2775S) (1672775S, Cell signaling Technology, USA) was used at a dilution of 1/1000 in PBS containing 2 mg/mL BSA and 0,02% sodium azide, with 5 mL applied per membrane.

The next day, membranes were washed twice with TBST (10 minutes each), followed by incubation with the secondary antibody (goat anti-rabbit IgG (H+L) HRP-conjugated (PI-1000-1, Vector Laboratories, USA)) diluted 1/7500 in TBST without sodium azide for 1 hour at room temperature. Membranes were then washed three times with TBST (10 minutes each) and image revealed using clarity western peroxide reagent and clarity western luminol/enhancer reagent (ECL) (#1705060, Bio-Rad, USA) chemiluminescent substrate. Equal volumes (2 mL each) of the substrate reagents were mixed and applied to the membrane. Signal detection was carried out by exposing the membrane to a chemiluminescence imaging system (ImageQuant LAS 4000).

After this, the membranes were washed three times for 10 minutes each with 1X TBST. The procedure was then repeated for the detection of additional proteins. The primary antibodies used were: LAMP-2A Polyclonal Antibody (AMC2) (51-2200, Thermo Fisher

Scientific, USA), SQSTM1/P62 (D1Q5S) Rabbit mAb (39749, Cell Signaling Technology, USA), GAPDH (14C10) Rabbit mAb (2118, Cell Signaling Technology, USA), Anti-APG5L/ATG5 antibody EPR1755(2) (ab108327, Abcam, UK) and β-Actin (13E5) Rabbit mAb (4970, Cell Signaling Technologies, USA). The same protocol for secondary antibody incubation and chemiluminescent detection was followed as described above.

To analyse the expression of proteins that have similar molecular weight, a stripping protocol was used to allow detection on the same membrane. First, the membranes were rinsed five times with distilled water to remove residual chemiluminescent substrate. Meanwhile, 10 mL of stripping buffer was preheated to 50 °C. The membranes were then incubated in the stripping buffer at 50 °C for 45 minutes in a dry incubator. After incubation, they were washed in tap water for 1 hour, replacing the water every 15 minutes to ensure complete removal of the stripping buffer. Finally, the membranes were washed in TBST 1X for 5 minutes before proceeding with the blocking for 1 hour.

The mentioned proteins analysed by Western blot were chosen as representative markers of MA and CMA, as well as for assessing autophagic flux. LC3 was used to evaluate MA activity; upon autophagy induction, cytosolic LC3-I is lipidated to form LC3-II, which incorporates into autophagosomal membranes (46, 47). To complement this, SQSTM1/P62 was analysed as a selective autophagy receptor that binds ubiquitinated protein aggregates and LC3. Its accumulation reflects impaired degradation, making it a useful indirect marker of lysosomal function (43, 47). ATG5, a protein essential for autophagosome elongation, was included to assess early MA induction (46). LAMP2A was included as the lysosomal receptor and rate-limiting component of CMA, responsible for mediating the selective translocation of cytosolic proteins that have KFERQ-like motif into the lysosomal lumen (39). Its expression is dynamically regulated and typically increases during prolonged fasting or cellular stress, making it a specific marker for CMA activation (39). GAPDH is a glycolytic enzyme and known CMA substrate, used to monitor its selective degradation during CMA activation (39) and β-Actin as a loading control for sample normalization.

By examining these markers, we aimed to obtain a comprehensive view of both MA and CMA pathways in MCF-7 cells following repeated fasting cycles.

2.7. Quantification of Protein Expression by Western blot

After the Western blot membranes were developed, the bands were quantified by plotting their intensity profiles using FIJI (ImageJ). For each sample, background signal was subtracted individually to correct for non-specific staining. Red Ponceau Staining was used to normalize the samples. Average between replicates and then relative expression values (Fold Change) were obtained for each protein and condition, comparing it to the biological relevance control condition, explained more thoroughly in the discussion. Standard deviation for each sample was calculated.

For **LAMP2A** (CMA marker) and **ATG5** (MA marker), comparisons were made only between fasting conditions and the fed control. Since these proteins are key components of autophagy machinery, including inhibitor-treated samples would not provide meaningful insights into their expression, as lysosomal inhibition affects degradation rather than protein induction.

In contrast, for **LC3**, **SQSTM1/P62**, and **GAPDH**, comparisons were made between inhibitor-treated and untreated samples under the same fasting condition. This allowed the evaluation of autophagic flux by assessing whether these substrates accumulated when lysosomal degradation was blocked.

2.8. Translational Perspective: Personalized Nutrition and Patient Care

In addition to the experimental procedures, this project included a translational component involving participation in clinical nutrition activities at IBIONS, a team specialized in personalized nutrition in collaboration with the Instituto Valenciano de Oncología (IVO). Consultations included a detailed dietary assessment, where patients were asked to describe their typical food intake, their interest in nutrition, and their awareness of how dietary improvements could influence treatment outcomes. Nutritional recommendations were tailored to each patient's treatment regimen and supported by current scientific evidence. Body composition was evaluated using bioimpedance analysis, and the clinical team followed each patient throughout the course of treatment, monitoring nutritional progress and adapting strategies based on observed improvements or changes.

3. Results

3.1. Cell Culture

The cell cultures progressed successfully throughout the experimental period, with MCF-7 cells showing stable growth, adherence, and viability under the conditions described in *materials and methods*. MCF-7 cells maintained their characteristic epithelial-like morphology (**Figure 4**). These features, together with the absence of significant spontaneous detachment or morphological alterations, confirmed the suitability of the cultures for subsequent fasting and autophagy modulation experiments, ensuring phenotypic stability and reproducibility.

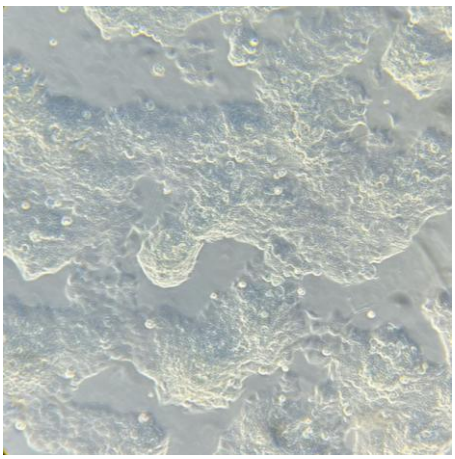

Figure 4. *MCF-7 cell culture at passage 11.*

3.2. IF in MCF-7 cells and Autophagy Modulation

To investigate the time-dependent activation of MA and CMA, two fasting protocols were applied in MCF-7 cells: a 4-hour serum starvation to trigger MA, and 16-hour fasting cycles followed by 8 hours of refeeding to promote CMA (34).

3.2.1. Microscopic Analysis of MCF-7 Cells under Experimental Conditions

3.2.1.1. Morphological Analysis of MCF-7 Cells under IF Cycles (MA experiment)

To initially see the impact of IF on BC cell viability and morphology, MCF-7 cells were observed under the Leica DMi1 Inverted Microscope after being subjected to different nutrient deprivation cycles to see MA activation (**Figure 5**). The fasting protocol consisted of a 4-hour serum starvation followed by 20 hours of complete growth medium, repeated up to three cycles depending on the condition.

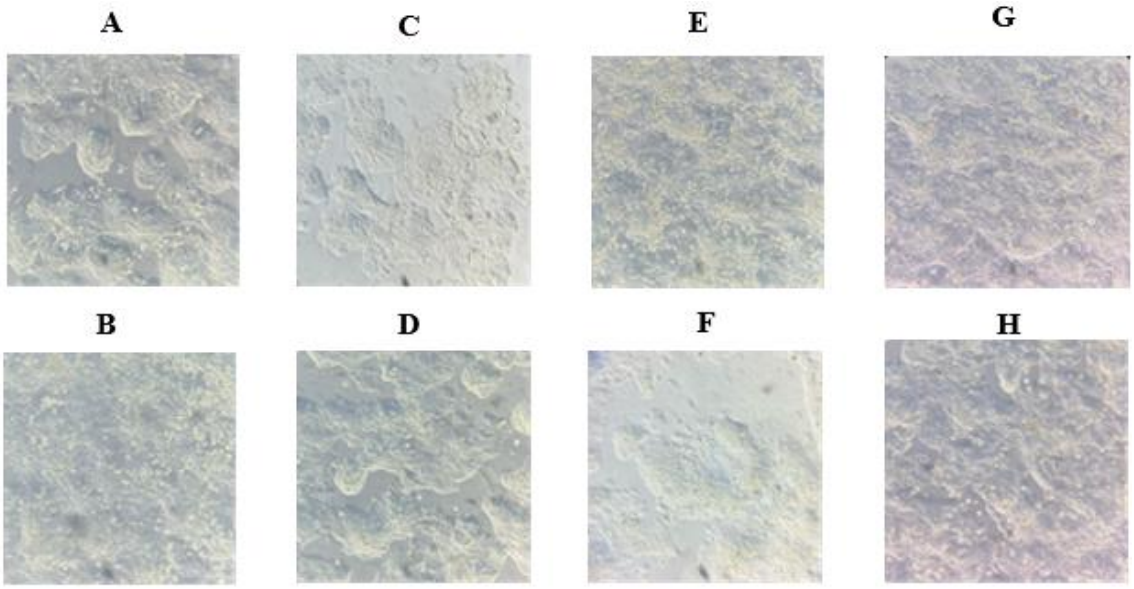

Figure 5. *Morphological appearance of MCF-7 cells under different IF conditions to induce MA. Cells were subjected to 0 (control), 1, 2, or 3 fasting cycles, consisting of 4 hours in serum-free medium followed by 20 hours in complete medium. Inhibitor conditions, NL (NH_4Cl 10 mM + leupeptin 150 μM) were applied during the last cycle.* ***A****. Control;* ***B****. Control + NL;* ***C****. 1 Fasting cycle;* ***D****. 1 Fasting cycle;* ***E****. 2 Fasting cycles;* ***F****. 2 Fasting cycles + NL;* ***G****. 3 Fasting cycles;* ***H****. 3 Fasting cycles + NL. Images taken under 10x objective.*

Under nutrient-rich control conditions (**Figure 5A**), cells exhibited typical epithelial-like morphology, forming a dense monolayer with no signs of detachment or cell death, establishing a baseline for subsequent comparisons. In the control + NL group (**Figure 5B)** cells retained similar confluency and morphology to the control, though a modest increase in unattached brighter cells (indicative of cell death) was observed. Following a single fasting cycle **(Figure 5C),** cellular density, shape, and adherence remained unchanged, mirroring control conditions. When combined with inhibitors (**Figure 5D**), cells displayed slight granularity but maintained overall morphology and confluency. Two fasting cycles (**Figure 5E**) introduced initial irregularities, with heterogeneous cell distribution (high- and low-density regions), though these changes were inconsistent across the well. The addition of inhibitors (**Figure 5F**) to two cycles had more pronounced effects: reduced cell density, detachment, and lighter fields suggestive of cell death. After three fasting cycles (**Figure 5G**), cells exhibited varied organizational patterns, including aggregation and rounding, a potential indicator of early stress or viability loss. Finally, three cycles combined with inhibitors (**Figure 5H**) resulted in alterations, including reductions in density, rounded cells, and disrupted adherence, indicating that prolonged fasting with autophagy inhibition synergistically compromises viability.

This progression highlights that morphological and viability changes appear with repeated fasting cycles, particularly when autophagy is inhibited, underscoring autophagy's potential protective role during nutrient stress.

This pattern was consistently observed across the remaining three replicates, supporting the reproducibility and robustness of the morphological observations.

3.2.1.2. Morphological Analysis of MCF-7 Cells under IF Cycles (CMA experiment)

In case of the CMA protocol, cells were subjected to 16-hour serum starvation followed by 8 hours of complete growth medium, repeated up to three cycles depending on the condition. Cells were observed (**Figure 6**) at same conditions as MA experiment.

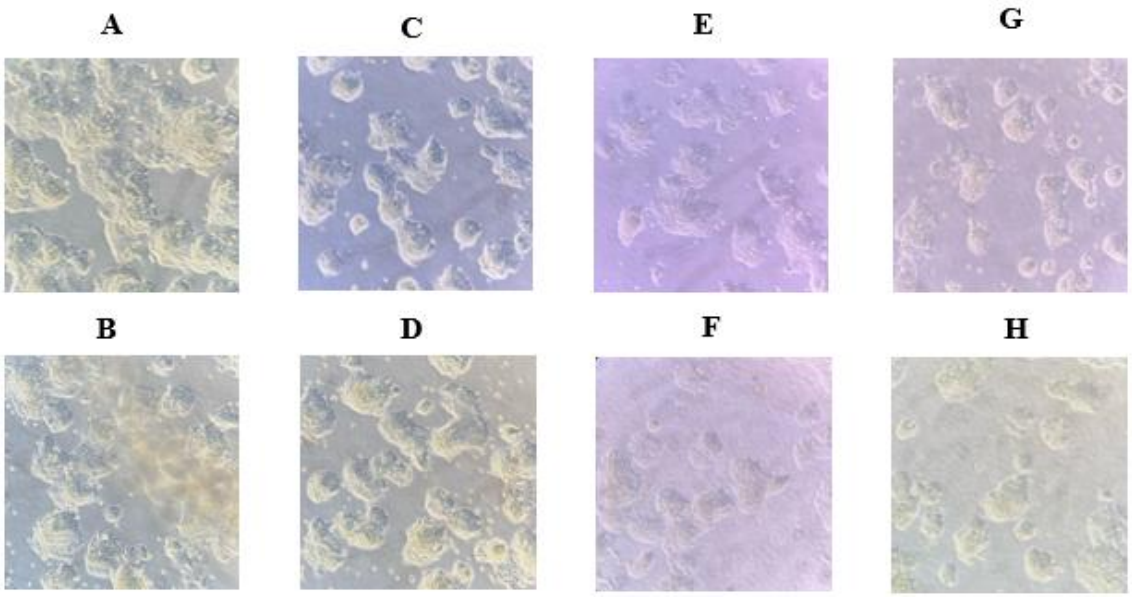

Figure 6. *Morphological appearance of MCF-7 cells under different IF conditions to induce CMA. Cells were subjected to 0 (control), 1, 2, or 3 fasting cycles, consisting of 16 hours in serum-free medium followed by 8 hours in complete medium. Inhibitor conditions, NL were applied during the last cycle.* ***A****. Control;* ***B****. Control + NL;* ***C****. 1 Fasting cycle;* ***D****. 1 Fasting cycle;* ***E****. 2 Fasting cycles;* ***F****. 2 Fasting cycles + NL;* ***G****. 3 Fasting cycles;* ***H****. 3 Fasting cycles + NL. Images were taken under 10x objective.*

Under control conditions (**Figure 6A**), cells maintained a healthy appearance, forming compact epithelial clusters with no visible signs of stress or death. In the control + NL group (**Figure 6B**), cellular morphology closely resembled that of the control, although a slight increase in rounded and unattached (brighter) cells was noted, without major alterations. Following a single fasting cycle (**Figure 6C**), cells remained well distributed and structurally intact, with no significant morphological differences from the control, the well had less cells from the beginning, there was no reduction in confluency. The addition

of inhibitors to one fasting cycle (**Figure 6D**) again preserved overall morphology; while a possible increase in intracellular granularity (potentially dead cells) was observed, confluency and cell shape remained comparable to fasting alone. With two fasting cycles (**Figure 6E**), visible changes became apparent: confluency was slightly reduced, and cells appeared more spaced and less compact. When inhibitors were combined with two fasting cycles (**Figure 6F**), cell density was decreased, and cells appeared thinner and more spread out, indicative of reduced adhesion or cell loss. After three fasting cycles (**Figure 6G**), confluency continued to decline, with some cells becoming more rounded and clusters less defined, overall morphology was generally preserved. In the three fasting cycles + NL (**Figure 6A**), similar changes to (**Figure 6F**) were noted, with an additional reduction in cell density, increased rounding, and more frequent cell detachment, consistent with diminished viability or heightened cellular stress.

So, repeated fasting cycles, particularly when autophagy is inhibited, progressively impact cell morphology and density, suggesting a cumulative effect on cellular health and survival.

This pattern was also observed in the other three replicates, confirming the reproducibility and consistency of the morphological changes across experiments.

3.2.2. Protein Quantification by Lowry Assay

Following the completion of IF stimuli in MCF-7 cells under both MA and CMA protocols, all samples were collected and lysed. To determine the total protein concentration in each condition and ensure accurate protein loading for Western blot analysis, a Lowry assay was performed using the protocol adapted for 96-well plates.

As there were 8 different samples (4 replicates of CMA and 4 replicates of MA), 2 plates were used to fit the duplicates (in plate 1: replicates 1 and 3 of CMA and MA; plate 2 replicates 2 and 4 of CMA and MA).

3.2.2.1. Standard Curve Generation

A standard curve was generated using known concentrations of BSA ranging from 0 to 20 µg per well. Each concentration was measured in duplicate and the average absorbance values were calculated. The resulting standard curve of plate 1 showed a linearity of R^2 = 0,9836, and the equation of the regression line was:

$$Absorbance_{675} = 0{,}0102 \times BSA\ (ug) + 0{,}0913$$

And the resulting standard curve of plate 2 (**Figure 7**) showed a linearity of $R^2 = 0.9876$, and the equation of the regression line was:

$$Absorbance_{675} = 0{,}0133 \cdot BSA\ (ug) + 0{,}0766$$

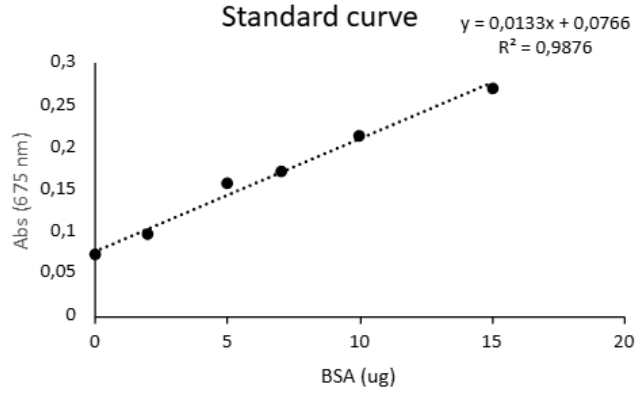

Figure 7. *Standard curve for BSA. Absorbance at 675 nm was measured for increasing concentrations of BSA. The curve was used to interpolate the protein concentration of experimental samples.*

3.2.2.2. Sample Absorbance and Averaging

Experimental samples (MCF-7 cell lysates) from different conditions were measured in duplicate. These included four CMA groups (Control, A1, A2, A3) and four MA groups (Control, A1, A2, A3).

The average absorbance for each duplicate was calculated and grouped by experimental condition (**Table 2**). Minor variations between duplicates were observed, indicating good reproducibility.

Table 2. *Average absorbance values for each condition and replicate.*

	Average (Abs 657nm)							
	CMA 1	**MA 1**	**CMA 3**	**MA 3**	**CMA 2**	**MA 2**	**CMA 4**	**MA 4**
Ct	0.2012	0.183	0.1786	0.1883	0.2738	0.2263	0.23275	0.2097
Ct+NL	0.1464	0.1985	0.2344	0.2294	0.2811	0.2419	0.1998	0.2141
A1	0.1535	0.2169	0.2135	0.2543	0.2077	0.2823	0.1877	0.1594
A1+NL	0.2054	0.1886	0.1495	0.2008	0.1789	0.2358	0.15755	0.2053
A2	0.1646	0.1729	0.1408	0.2436	0.2069	0.2402	0.12925	0.1305
A2+NL	0.1523	0.2137	0.2021	0.1967	0.2231	0.2110	0.15025	0.1960
A3	0.1263	0.1835	0.1529	0.2241	0.2034	0.1699	0.1285	0.1585
A3+NL	0.1296	0.1623	0.1419	0.2128	0.2481	0.1546	0.14905	0.1557

3.2.2.3. Protein Concentration Calculation

Using the equation obtained from the standard curve, protein concentrations in µg/µL were determined for each sample. This allowed the determination of exact protein content for each sample replicate.

3.2.2.4. Sample Volume Adjustment for Western Blot

To load equal amounts of protein (20 µg) per lane, sample-specific volumes were calculated based on each concentration. As 4X loading buffer was used, 4 µL were added for a total volume of 16 µL. Based on the volume of lysate needed to reach 20 µg, the remaining volume was completed with distilled water.

This normalization ensures consistent protein loading across all experimental conditions in the following SDS-PAGE and Western Blot analysis.

3.2.3. Protein Detection by Western Blot

Western blot analysis was preformed to evaluate the expression levels of key proteins involved in autophagy through MA and CMA in MCF-7 cells exposed to different fasting cycles.

During the internship period, and due to the novelty of the project, several technical aspects including fasting induction, cell lysis and protein quantification had to be newly established. The laboratory infrastructure had recently been established, which required the setup and validation of procedures from the beginning, and protocols for Western blotting, antibody dilutions, and membrane handling required optimization. Therefore, time only allowed the Western blot analysis of the first two biological replicates (n=2) for both MA and CMA conditions. Additional replicates will be analysed in future experiments to complete the dataset and strengthen the conclusions and have statistical reliability.

3.2.4. Quantification of Protein Expression by Western Blot

Expected molecular weight were approximately 18-16 kDa for LC3 (LC3-I cytolytic, 18 kDa, and LC3-II membrane-bound, 16 kDa), 50-60 kDa for SQSTM1/P62, 46 kDa (or 100 kDa when glycosylated) for LAMP2A, 36 kDa for GAPDH and 55 kDa for ATG5.

Each Western blot was performed using lysates from MCF-7 cells subjected to one, two, or three fasting cycles (A1 to A3), with their respective fed controls (C), and with or without lysosomal inhibitors (NH_4Cl + leupeptin, denoted as “i”). Due to sample loss

during lysis in one replicate (CMA n1), data for A3 and A3+i in that set could not be obtained.

All samples were normalized to 20 µg of total protein and loading consistency was verified by Ponceau S staining (**Annex A1**) prior to antibody incubation. Results are presented as mean ± standard deviation (SD) from two biological replicates (n = 2). I acknowledge that a minimum of three biological replicates is typically required for robust statistical analysis; however, due to the experimental constraints discussed above, it was not possible to complete a higher number of replicates within the framework of this thesis. Further work is ongoing at this moment to expand the sample size.

All values are expressed as fold change relative to the described control: for LAMP2A and ATG5 relative to the fed control, and for SQSTM1/P62, LC3, and GAPDH, inhibited versus non-inhibited conditions. Bars represent mean ± standard deviation of n = 2 biological replicates.

3.2.4.1. Quantification of 4-hour Fasting Condition Samples (MA)

Signal intensities were normalized. In all membranes except the 15% gel membrane used for LC3 analysis, normalization was performed using Ponceau S staining, which accounts for total protein load. For LC3, normalization was done against β-actin (loading control), as Ponceau staining image did not allow accurate quantification.

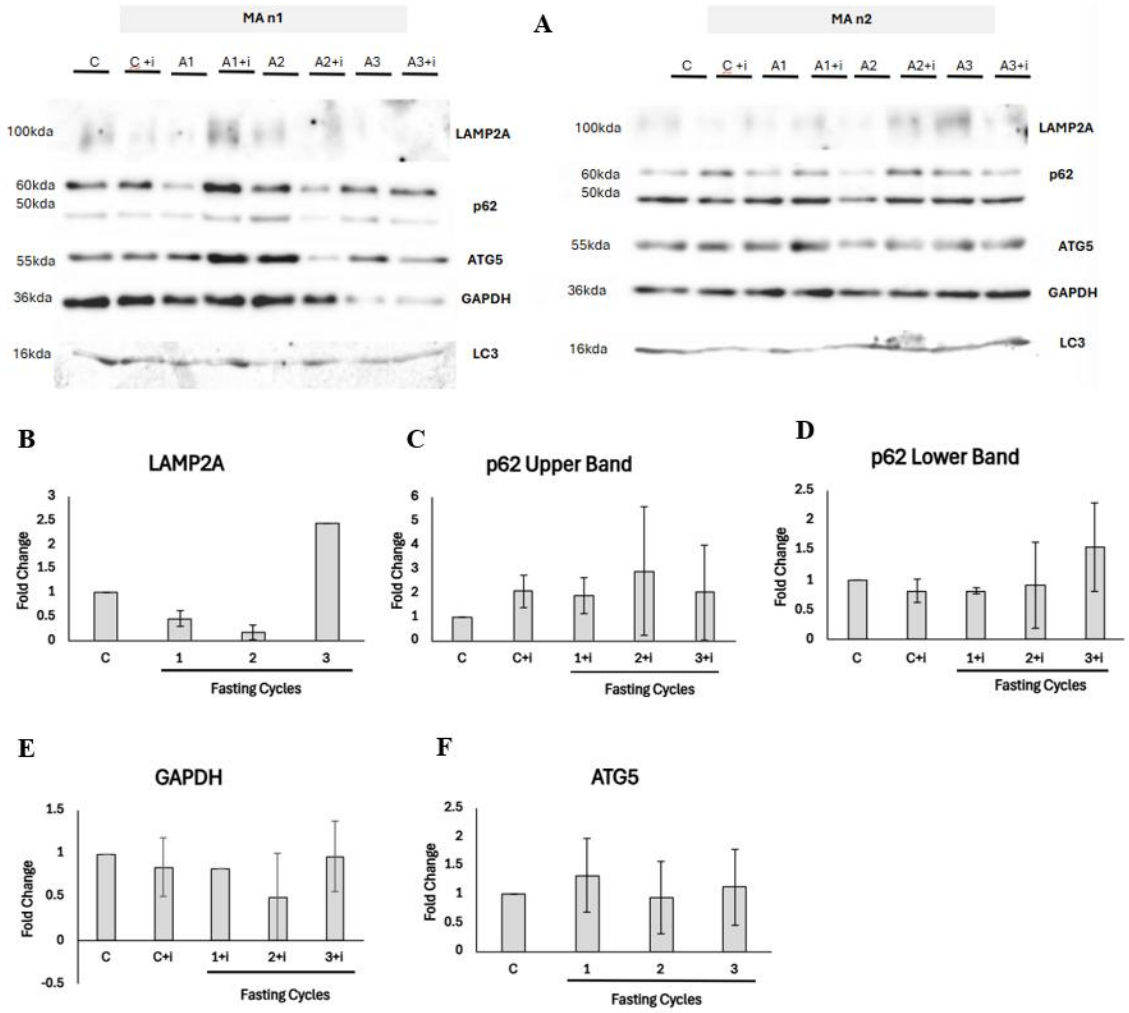

Figure 8. *Western blot analysis and quantification of autophagy-related proteins under 4-hour fasting cycles and lysosomal inhibition conditions in MCF-7 cells.* ***(A)*** *Representative Western blots from two independent replicates (MA n1 and MA n2) using 12% SDS-PAGE membranes. Protein expression of LAMP2A, SQSTM1/P62, ATG5, GAPDH, and LC3 was evaluated in control cells (C), after 1, 2, or 3 cycles of fasting (A1–A3), and in their corresponding conditions with lysosomal inhibitors (i).****(B–F)*** *Quantification of fold change relative to appropriate controls for each protein and condition:* ***(B)*** *LAMP2A,* ***(C)*** *P62 upper band,* ***(D)*** *P62 lower band,* ***(E)*** *GAPDH, and* ***(F)*** *ATG5. Data are presented as mean ± standard deviation from two replicates.*

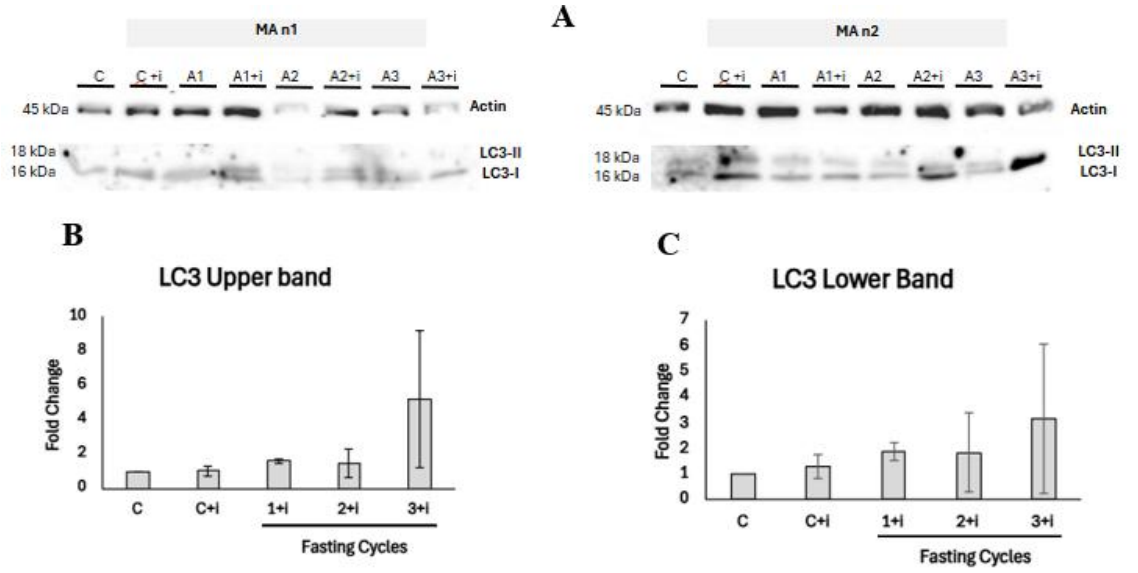

Figure 9. *Western blot analysis and quantification of LC3 expression to evaluate macroautophagy under 4-hour fasting conditions with or without lysosomal inhibition in MCF-7 cells.* ***(A)*** *Western blot results from two independent replicates (MA n1 and MA n2) performed on 15% SDS-PAGE gels, showing LC3-I and LC3-II protein levels, with β-actin used as loading control. Samples include control (C), 1, 2, or 3 cycles of fasting (A1–A3), and their corresponding conditions with lysosomal inhibitors (+i).* ***(B–C)*** *Fold change quantification of* ***(B)*** *LC3-II (upper band) and* ***(C)*** *LC3-I (lower band) levels relative to the appropriate controls for each condition. Data are presented as mean ± standard deviation from two replicates.*

As we can see in **Figure 8A**, in both replicates (MA n1 and MA n2), LAMP2A bands appeared faint and diffuse across all lanes, with limited signal intensity that made detection difficult. ATG5 and GAPDH bands were clearly defined and consistently loaded across samples, showing comparable intensity. In the case of SQSTM1/P62, signal appeared as double band between 50-60 kDa in both replicates. Interestingly, in replicate 1, the upper band shows more intensity, while in replicate 2, the lower one does.

For LC3, the 12% acrylamide gels used in the first set of blots (**Figure 8A**) did not allow clear separation of the LC3-I and LC3-II isoforms, resulting in faint or merged bands. To address this, additional blots were run on 15% acrylamide gels, where improved resolution was achieved (**Figure 9A**). In these membranes, both isoforms (LC3-I ~16 kDa and LC3-II ~18 kDa) could be distinguished more clearly, particularly in MA n2. The signal was notably stronger in the inhibitor-treated conditions, especially A2+i and A3+i. Although, in this case, β-actin was used (expected molecular weight: 45 kDa) as a loading control since the Red Ponceau S did not provide a sufficiently clear image for normalization, it is important to note that total protein stains such as Ponceau S is generally preferred over housekeeping proteins like β-actin, especially in experiments

involving autophagic flux (48). This is because Ponceau S provides a more accurate and consistent reference across samples and is not affected by potential changes in housekeeping protein expression that may occur under cellular stress or autophagy induction (48). Furthermore, actin showed uniform intensity across all samples, supporting consistent sample loading (**Figure 9A**).

For CMA markers**,** LAMP2A (**Figure 8B**) expression decreased after one and two fasting cycles compared to the fed control, while a marked increase was observed after three cycles, with a fold change above 2.5. The standard deviation (SD) was low across all conditions. Regarding GAPDH (**Figure 8E**), levels remained relatively stable across all fasting conditions except for "2+i," which showed a decrease. When comparing fasting cycles with and without inhibitor, all had a fold change <1. No major changes were detected, but variability between replicates was high.

On the other hand, MA markers showed for LC3, both the upper **(Figure 9B)** and lower (**Figure 9C**) bands showed progressive accumulation in the presence of the inhibitor as the number of fasting cycles increased. The most pronounced increase was observed in the upper band after three cycles (LC3-II), with a fold change close to 5, while the lower band (LC3-I) reached a fold change close to 3, though with substantial variability. Both bands followed a similar trend, but the lower band exhibited less intensity. Regarding SQSTM1/P62, both the upper and lower bands were analysed. In the upper band (**Figure 8C**), treatment with the inhibitor led to increased protein levels in all conditions compared to the corresponding fasting cycle without inhibitor, particularly after two cycles, although the SD was high. In the lower band (**Figure 8D**), more moderate increases were observed, with a gradual rise across fasting cycles and the highest values after three cycles. Finally, for ATG5 (**Figure 8F**), no significant changes were observed across the fasting cycles, as expression levels remained similar to the fed control in most conditions, but >1. However, error bars were relatively large.

3.2.4.2. Quantification of 16-hour Fasting Condition Samples (CMA)

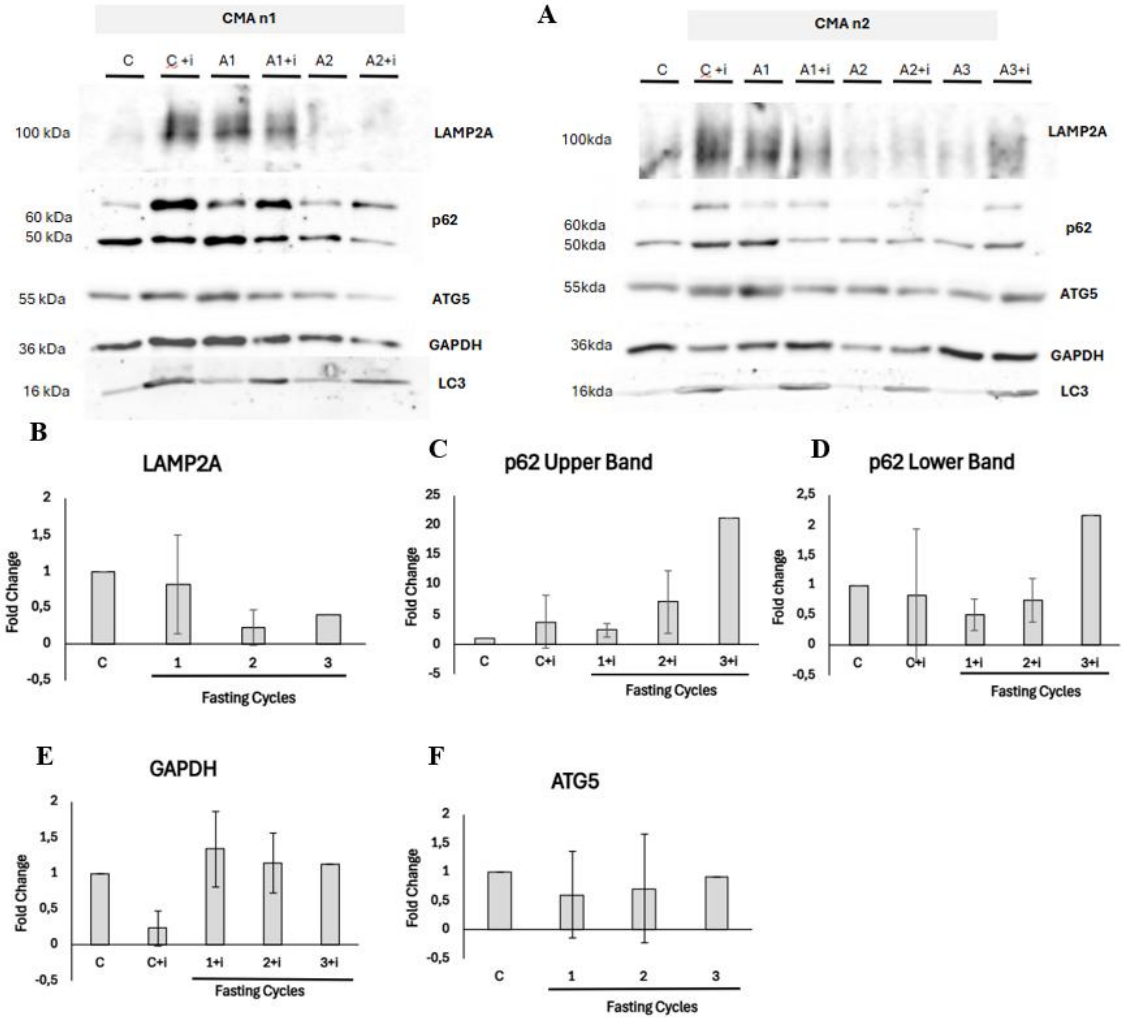

Figure 10. *Western blot analysis and quantification of autophagy-related proteins under 16-hour fasting cycles and lysosomal inhibition conditions in MCF-7 cells.* ***(A)*** *Representative Western blots from two independent replicates (CMA n1 and CMA n2) using 12% SDS-PAGE membranes. Protein expression of LAMP2A, SQSTM1/P62, ATG5, GAPDH, and LC3 was evaluated in control cells (C), after 1, 2, or 3 cycles of fasting (A1–A3), and in their corresponding conditions with lysosomal inhibitors (i).* ***(B–F)*** *Quantification of fold change relative to appropriate controls for each protein and condition:* ***(B)*** *LAMP2A,* ***(C)*** *P62 upper band,* ***(D)****P62 lower band,* ***(E)*** *GAPDH, and* ***(F)*** *ATG5. Data are presented as mean ± standard deviation from two replicates.*

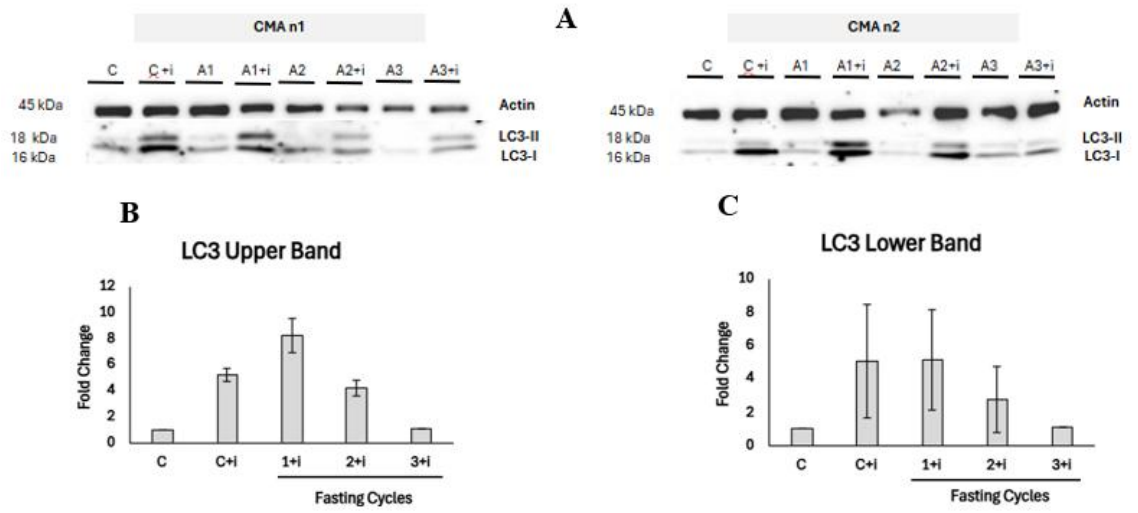

Figure 11. *Western blot analysis and quantification of LC3 expression to evaluate macroautophagy under 16-hour fasting conditions with or without lysosomal inhibition in MCF-7 cells.* ***(A)*** *Western blot results from two independent replicates (CMA n1 and CMA n2) performed on 15% SDS-PAGE gels, showing LC3-I and LC3-II protein levels, with β-actin used as loading control. Samples include control (C), 1, 2, or 3 cycles of fasting (A1–A3), and their corresponding conditions with lysosomal inhibitors (+i).* ***(B–C)*** *Fold change quantification of* ***(B)*** *LC3-II (upper band) and* ***(C)*** *LC3-I (lower band) levels relative to the appropriate controls for each condition. Data are presented as mean ± standard deviation from two replicates.*

In **Figure 10A** LAMP2A bands appeared variable and faint in both n, particularly in CMA n2 A3+i, where the signal was barely detectable. Overall, the intensity and definition of LAMP2A was inconsistent. SQSTM1/P62 was detected as a clear double band around 60–50 kDa in all conditions, with visibly stronger signal in the inhibitor-treated samples, especially in CMA n2. ATG5 showed stable and well-defined expression across samples, with consistent band intensity and good resolution. GAPDH bands were strong and uniform in most conditions, although slightly reduced in intensity in some inhibitor-treated lanes.

In the case of LC3, the initial blots run on 12% acrylamide gels did not allow clear resolution of LC3-I and LC3-II isoforms (**Figure 10A**), resulting in faint or merged bands. To improve separation, LC3 was reanalysed on 15% gels (**Figure 11A**). These membranes provided much clearer distinction between LC3-I (~16 kDa) and LC3-II (~18 kDa), particularly in CMA n2, where increased signal was observed in inhibitor-treated conditions. Actin was used as a loading control and showed consistent intensity across most of the samples (despite n2 A2 where it was low) supporting proper protein normalization.

For CMA markers**,** LAMP2A (**Figure 10B**) levels slightly decreased after one and two fasting cycles and showed a small increase at three cycles; however, none of the conditions exceeded the baseline control level (C). The SD was notably high in the 1-cycle group. Regarding GAPDH (**Figure 10E**), increased levels were observed under fasting cycles and in inhibitor-treated conditions, while levels decreased in the fed condition with inhibitor. The SD for GAPDH was moderate in most conditions.

Regarding MA markers**,** LC3-II (upper band) (**Figure 11B**), expression increased notably in conditions with lysosomal inhibitors, especially at "1+i", where the fold change exceeded 8. As the number of cycles increased, the fold change relative to the control decreased compared to "1+i", but remained higher than the control. The SD was acceptable overall, with the highest variability observed in "C+i" and "1+i". LC3-I (lower band) (**Figure 11C**) followed a similar pattern, with increased intensity under lysosomal inhibition, particularly in "1+i" and "2+i". The SD for LC3-II was relatively high in "C+i" and "1+i". For SQSTM1/P62 (upper band) (**Figure 10C**), a marked accumulation was observed in conditions with NL, with the most prominent increase in the "3+i" condition, where the fold change reached approximately 20. The SD was larger in conditions "2+i" and "C+i". For SQSTM1/P62 (lower band) (**Figure 10D**), a progressive accumulation was observed with lysosomal inhibitors at "3+i", while levels decreased in "1+i" and "2+i". The SD was moderately high in most conditions. Finally, ATG5 (**Figure 10F**) expression remained relatively stable across all fasting conditions, with all groups showing values close to the control, but <1. The SD was considerable in fasting conditions, especially in "1+i" and "2+i".

All values are expressed as fold change relative to the described control mentioned before: for LAMP2A and ATG5 relative to the fed control, and for SQSTM1/P62, LC3, and GAPDH, inhibited versus non-inhibited conditions. Bars represent mean ± standard deviation of n = 2 biological replicates.

3.3. Translational Perspective: Personalized Nutrition and Patient Care

In parallel with the experimental laboratory work conducted at the Department of Preventive Medicine and Public Health at the of Valencia, this undergraduate thesis also included a practical immersion in translational research and patient-centred care. Specifically, I participated in activities at **IBIONS**, specialized in personalized nutrition for oncology patients, which collaborates directly with the IVO. IBIONS is responsible

for the nutritional support of patients with BC treated at IVO, implementing strategies tailored to each individual's clinical profile, metabolic status, and treatment response.

My involvement surrounded several aspects of knowledge translation, actively contributing to nutritional consultations and informative workshops for oncology patients, promoting awareness of how evidence-based dietary interventions can serve as adjuvants to conventional therapies. Furthermore, I participated in literature bibliography and scientific discussions focused on the emerging role of nutrition in modulating treatment efficacy and quality of life in cancer care.

Finally, as part of my commitment to research and ongoing training, I participated in the *IX Trobada d'investigadors i investigadores en càncer Ciutat d'Alcoi: Impulsando la Vida. Metabolismo, Ejercicio y Nutrición Contra el Cáncer.* This experience allowed me to stay informed about the latest advances in metabolism, nutrition, and physical exercise in cancer patients, and contributed to broadening my perspective on the impact of these factors in cancer prevention and quality of life improvement for affected individuals. Some of the talks that I want to give special attention are the one from Marcos Malumbres, where he talked about the importance of prevention, and Antonia Tomás Loba, who talked about the disruption of circadian rhythms. Additionally, the past 27th of May I listened to Ana Maria Cuervo's talk in the commemorative lection Jiménez Díaz, an expert in the field of autophagy, especially CMA.

Through this dual experience, research and patient-centred nutritional intervention, this thesis integrates basic molecular insights with clinical applicability, highlighting the relevance of **personalized nutrition as a translational bridge** between laboratory findings and the improvement of real-world patient outcomes.

4. Discussion

The main objective of this project was to determine if repeated cycles of fasting could modulate differentially the activation of autophagy (MA and CMA in ER+ BC (MCF-7)). Even though that the obtained results are not statistically significant due to low n (n=2), a descriptive analysis enables to extract some tendencies and interesting reflections.

To assess the activation of autophagy under different fasting conditions, key markers of MA and CMA, selected based on their functional roles and relevance in literature, were evaluated to observe autophagic flux and lysosomal degradation.

Importantly, the autophagic flux, reflects the dynamic process of autophagy from initiation to lysosomal degradation. To evaluate it, lysosomal inhibitors were applied only during the last fasting cycle of each condition, NH_4Cl raises lysosomal pH, inhibiting acid-dependent hydrolases, while leupeptin blocks cysteine and serine proteases such as cathepsins (43). When combined, these agents effectively impair lysosomal degradation. Comparing protein levels in samples with and without inhibitors enables the detection of whether an observed accumulation is due to increased autophagy induction or defective degradation (43). This is especially relevant for LC3-II, SQSTM1/P62, and GAPDH, whose stabilization under lysosomal inhibition indicates active flux (42).

LC3 was used to monitor autophagosome formation, as the accumulation of the lipidated form, LC3-II, is considered a hallmark of MA activation. According to current autophagy guidelines (43), quantification of LC3-II levels, comparing samples treated with versus without lysosomal inhibitors provides a more accurate estimate of autophagic flux than comparing LC3-I and LC3-II bands directly (43). In the initial experiment, separation of LC3 isoforms was suboptimal in 12% SDS-PAGE gels but was improved in 15% gels due to their smaller pore size. In our MA experiments (4-hour fasting), LC3-II flux increased progressively with each fasting cycle, indicating enhanced autophagic flux. This is consistent with the well-established notion that MA is rapidly induced in response to nutrient deprivation, serving as an immediate adaptive mechanism to maintain cellular homeostasis (42). Contrary, under the CMA protocol (16-hour fasting), LC3-II flux tended to decrease with repeated fasting. This divergent likely reflects the compensatory and often inhibitory relationship described between MA and CMA. Several studies have shown that when one autophagic pathway is active, such as CMA during prolonged fasting, MA activity can be downregulated as a compensatory mechanism, and vice versa (35, 39). Therefore, while LC3-II flux increases progressively with the number of short fasting cycles, it decreases when fasting duration is extended, consistent with a shift in autophagic preference from MA to CMA (43). This dual behaviour of LC3-II supports the concept of mutual compensation and inhibitory crosstalk between the two pathways (43). However, further studies with higher statistical power are needed to confirm this relationship in our model. Additionally, implementing genetic inhibition strategies, such as siRNA-mediated knockdown of key proteins like ATG5 for MA or LAMP2A for CMA, could help to understand the relationship between these pathways during nutrient

deprivation and clarify whether their activities are mutually exclusive, sequentially regulated, or context-dependent (49, 50).

Regarding SQSTM1/P62, it was used as a marker of autophagic flux, since its accumulation indicates impaired degradation of autophagic cargo by lysosomes. SQSTM1/P62 appeared as two distinct bands: the upper band (60 kDa) is often associated with post-translational modifications, particularly ubiquitination, while the lower band (50 kDa) represents the non-modified form (51). This distinction is important because ubiquitinated SQSTM1/P62 plays a critical role in selective autophagy by binding to ubiquitinated substrates and LC3-II on autophagosomal membranes (52). In MA experiments (4-hour fasting), the upper band showed and increased flux progressively as the number of fasting cycles increased, while the lower band showed a significant increase only after the third cycle. This differential response suggests that early in the fasting response, SQSTM1/P62 may undergo increased ubiquitination to facilitate selective autophagy, while the SQSTM1/P62 flux increases more substantially with prolonged fasting stress (52). However, the high variability observed in these samples indicates that additional studies are needed to confirm this pattern. In CMA protocol (16-hour fasting), both the upper band and lower band showed a pattern similar to the MA experiment, with the upper band increasing with more cycles and the lower band only showing levels higher than control in the third cycle. This parallel response in both protocols suggests that its accumulation might be a common feature of repeated fasting (53). The increased accumulation of ubiquitinated SQSTM1/P62 (upper band) with repeated fasting cycles may reflect cellular adaptation to nutrient stress, as cells upregulate selective autophagy mechanisms to target specific substrates for degradation (54). Meanwhile, the delayed increase in non-modified SQSTM1/P62 (lower band) could indicate a secondary response when selective mechanisms become overwhelmed, leading to more generalized autophagy activation (53). In addition to its well-known degradation via MA, SQSTM1/p62 could also be targeted for proteasomal degradation, as shown by its accumulation upon MG132 treatment (55). Moreover, although SQSTM1/p62 is not currently recognized as a classical CMA substrate, it remains to be determined whether it contains a KFERQ-like motif. Future sequence analysis would be useful to assess whether CMA could contribute to its degradation under prolonged nutrient stress. These findings support the concept of dynamic cross-talk between different autophagic pathways during nutrient deprivation (39). However, the high variability in our samples underscores the

need for additional replicates and more robust statistical analysis to fully elucidate these patterns and their biological significance.

As for ATG5, it is a key protein involved in the early steps of autophagosome formation. It forms a complex with ATG12 and ATG16L1, which together help build and close the autophagosomal membrane (28, 43). ATG5 levels provide insight into the autophagosome initiation capacity, making it a relevant marker for studying MA (39). In our experiments, ATG5 levels remained remarkably stable across all conditions, with fold change values very close to 1 in both MA and CMA protocols. In the MA (4-hour fasting) experiment, ATG5 levels were slightly above 1, while in the CMA (16-hour fasting) protocol, they were slightly below 1, but with high standard deviation in the CMA samples. This lack of substantial change could suggest that the initiation machinery of autophagy was not significantly modulated by repeated fasting cycles in our model. This observation is consistent with previous reports indicating that ATG5 expression is often maintained at basal levels, and that the regulation of autophagic flux in response to nutrient deprivation or stress typically occur downstream, at the level of autophagosome maturation, cargo recognition or lysosomal degradation (28, 43). In certain contexts, autophagic activity can be up- or downregulated without significant changes in the expression of core autophagy proteins such as ATG5, especially when compensatory mechanisms between MA and CMA are active (39). Additionally, high variability observed in the CMA protocol may be due to technical factors, such as inconsistent cell seeding or pipetting errors, or biological variability within the samples. This highlights the need for increased replicate numbers and more rigorous methodological controls in future studies to clarify whether subtle changes in ATG5 could play a role in the interplay between MA and CMA under repeated fasting conditions.

As for LAMP2A, key receptor for CMA at the lysosomal membrane. It mediates the selective translocation of cytosolic proteins containing a KFERQ-like motif into the lysosome for degradation (15, 39), its levels are tightly regulated and are considered the rate-limiting factor for CMA activity, making it a central marker for monitoring changes in this pathway. In our experiments it showed a faint band which may reflect suboptimal antibody binding or low expression under these conditions. Still, when Fold change was analysed LAMP2A expression showed a dynamic pattern depending on the autophagy protocol. In the MA protocol (4-hour fasting), LAMP2A levels decreased as more cycles were done (in the third cycle we can see a big increase, likely due to high inter-sample

variability, as suggested by the elevated standard deviation), suggesting that short-term nutrient deprivation does not impact CMA activity. This is consistent with the literature, which indicates that MA is the predominant form of autophagy activated during shorter fasting, while CMA is more responsive to prolonged ones (39). Although not expected, under the CMA protocol (16-hour fasting), LAMP2A levels showed a decrease as the number of fasting cycles increased, with a notable high SD in these samples. The variability observed in LAMP2A levels, particularly in the CMA protocol, may also be influenced by technical factors such as sample handling, loading inconsistencies, or biological heterogeneity. This highlights again the importance of increasing replicate numbers and improving methodological consistency in future studies to clarify the regulatory dynamics of LAMP2A and CMA during fasting. Given that LAMP2A is the rate-limiting receptor for CMA, and that CMA is typically activated in response to prolonged or repeated stress such as extended fasting, it was expected that LAMP2A expression would increase as the number of fasting cycles increased. This would reflect the cell's adaptation to ongoing nutrient deprivation and the need for selective protein degradation via CMA (39).

Finally, GAPDH is a classical glycolytic enzyme, but in the context of autophagy studies, it is also recognized as a well-established substrate of CMA (35, 39). During CMA activation, GAPDH is selectively recognized by HSC70 and delivered to the lysosome for degradation via LAMP2A. Monitoring its flux can therefore provide insight into CMA activity, with decreased GAPDH flux indicating enhanced CMA-mediated degradation. In our experiments, GAPDH flux remained relatively stable across all conditions, with fold change values close to 1 in both MA and CMA protocols. In the MA (4-hour fasting) experiment, GAPDH flux were slightly above 1, while in the CMA (16-hour fasting) protocol, they were slightly below 1, but with high SD in the CMA samples. This lack of consistent change suggests that, under our experimental conditions, CMA-mediated degradation of GAPDH was not strongly induced, or that other compensatory mechanisms may have maintained its steady-state levels. This observation could be consistent with previous findings showing that CMA activation can be highly substrate- and context-dependent (35, 39). In some models, robust CMA activation leads to a marked decrease in GAPDH, but in others, especially where MA is also active, GAPDH levels may remain more stable due to compensatory degradation pathways or transcriptional upregulation (39). Alternatively, the lack of change between cycles and

high variability in the CMA protocol may reflect technical factors such as uneven cell seeding or pipetting errors, or biological variability within the samples. This highlights the need for increased replicate numbers and improved methodological consistency in future studies to clarify the regulatory dynamics of GAPDH and CMA during fasting. Given that GAPDH is a classical CMA substrate, its flux was expected to decrease with increased cycles of prolonged fasting, reflecting enhanced CMA activity (35, 39).

Overall, the results, even though low statistical significance, suggest a gradual activation of autophagy as fasting cycles increase. While MA markers, LC3 and SQSTM1/P62, responded more rapidly and showed stronger changes, CMA-related proteins (LAMP2A and GAPDH) showed more variable and less defined patterns. This supports the notion that different autophagy types are activated at distinct time scales and that repeated fasting may be more effective in promoting autophagic activity, particularly in ER+ BC cells (25, 35). These preliminary findings are consistent with previous results, which showed that prolonged caloric restriction reduced the incidence of chronic diseases, including lymphomas (the most common type of tumors in mice) (56).

These preliminary results suggest that performing three fasting cycles may enhance both MA and CMA activation more effectively than a single intervention in ER+ BC cells. As discussed in the introduction, this observation may hold relevance in the context of obesity, where the TME is characterised by chronic inflammation, altered macrophage plasticity, and resistance to immunotherapy. Modulating autophagy through fasting could contribute to TME reprogramming and improve immune responsiveness in these immunologically "cold" tumors, and this results could suggest that autophagy modulation through fasting could be a tool to change the immunosuppressor phenotype (31, 57). To translate these findings into clinical relevance, future studies should increase experimental rigor by expanding the number of replicates, incorporating *in vivo* models, and assessing the functional consequences of autophagy modulation on cell viability, immune response, and macrophage polarization. To accurately assess the potential of fasting cycles as a coadjuvant strategy in obesity-associated ER+ tumors, this comprehensive approach is required, potentially contributing to the reprogramming of the TME and enhancing responsiveness to standard therapies.

Several technical limitations must be acknowledged in this project. One of the main issues was sample variability between replicates. In the microscopy analysis, this was likely caused by initial variations in cell seeding density between wells, which resulted in

inconsistent confluency despite using a Neubauer chamber for cell counting. In Western blot analysis, variability was likely due to technical challenges related to protein extraction or gel loading. Additionally, some Western blot signals, particularly for LAMP2A, were faint or difficult to interpret, possibly due to suboptimal antibody performance, low protein expression, or sample degradation during the lysis process. In one of the replicates (MA n1), two samples (A3 and A3+i) were lost and could not be analysed. Finally, only two biological replicates were completed due to time and experimental constraints. While certain expression patterns were consistent, a greater number of independent experiments would be necessary to draw more robust and statistically sound conclusions.

Finally, it is important to contextualize this work within the setting in which it was developed. This project was carried out at the recently established Laboratory of Autophagy and Oncological Nutrition at the University of Valencia, under the supervision of Dr. Julio Madrigal Matute, who initiated this research line in the Department of Preventive Medicine in the current academic year. As a result, many experimental protocols, resources, and workflows were being implemented from scratch. Together with a master's student, I was among the first to contribute to the lab's foundation. This limited the number of replicates and experimental outputs within the timeframe of the thesis, which could be seen as a constraint in terms of data volume. However, it also provided a unique opportunity for scientific growth: I had significant autonomy in experimental design, literature searches, and the presentation of ideas. These efforts led to my participation in the Alcoy research congress and attendance at a talk by Dra. Ana Maria Cuervo, the researcher who discovered CMA, providing exceptional insight into the field.

In parallel, I had the chance to interact directly with breast cancer patients through IBIONS, applying the scientific knowledge acquired to clinical nutrition. This integration of bench and bedside not only enriched my understanding of translational research but also reinforced the importance of personalized nutrition as a tool for improving patient care in oncology. Therefore, beyond the experimental results, this experience contributed meaningfully to my scientific training and my ability to communicate and apply research findings in real-world settings

5. Future Perspectives

To deepen our understanding of how IF modulates autophagy in ER+ BC, future studies should first focus on increasing the number of biological replicates to strengthen statistical robustness and address variability. Additionally, incorporating complementary functional assays, such as assessments of cell viability, metabolic stress, apoptosis, or inflammatory markers, would help to explain the biological consequences of modulating MA and CMA. Building on the long-term goal of reprogramming the TME, future experiments should explore whether IF can restore CMA functionality in the context of obesity-induced dysregulation, shift macrophage polarization toward antitumor (M1-like) phenotypes, and reduce proangiogenic signalling pathways. This would involve evaluating the expression of key factors such as ICAM-1, VEGF, and cytokines within the TME. Moreover, validating these observations in *in vivo* models of obesity-associated ER+ BC will be crucial to assess whether repeated fasting cycles can turn immunologically "cold" tumors into "hot" ones, potentially enhancing their responsiveness to immunotherapy. Ultimately, this line of research may support the use of IF as a coadjuvant strategy to improve outcomes in patients who do not respond to standard treatments and lay the foundation for incorporating personalized nutritional interventions into integrative oncology approaches.

6. Conclusion

This project explored the activation of MA and CMA in ER+ BC cells exposed to different IF protocols. Through the design and implementation of a model comparing one, two, and three fasting cycles, it was possible to observe a trend towards increased autophagic activity as the number of cycles progressed, although this effect was more evident for MA-related proteins. These observations align with the initial hypothesis that repeated fasting enhances autophagy. The methodological approach allowed for the comparison of different fasting durations and their temporal effects on autophagy, the analysis of protein expression, and the use of lysosomal inhibitors to evaluate flux. Beyond the laboratory, the work was enriched by direct engagement with clinical nutrition practices in oncology, emphasizing the value of integrating molecular research with a translational perspective. Altogether, the project contributes to understanding how fasting duration may influence autophagy dynamics in ER+ BC cells, especially within the context of obesity, and opens the door for future investigations with greater statistical power.

7. Bibliography

1. Sung H, Ferlay J, Siegel RL, Laversanne M, Soerjomataram I, Jemal A, et al. Global Cancer Statistics 2020: GLOBOCAN Estimates of Incidence and Mortality Worldwide for 36 Cancers in 185 Countries. CA Cancer J Clin. 2021;71(3):209-49.
2. Lopez-Abente G, Mispireta S, Pollan M. Breast and prostate cancer: an analysis of common epidemiological features in mortality trends in Spain. BMC Cancer. 2014;14:874.
3. Kashyap D, Pal D, Sharma R, Garg VK, Goel N, Koundal D, et al. Global Increase in Breast Cancer Incidence: Risk Factors and Preventive Measures. Biomed Res Int. 2022;2022:9605439.
4. Bray F, Ferlay J, Soerjomataram I, Siegel RL, Torre LA, Jemal A. Global cancer statistics 2018: GLOBOCAN estimates of incidence and mortality worldwide for 36 cancers in 185 countries. CA Cancer J Clin. 2018;68(6):394-424.
5. Orrantia-Borunda E, Anchondo-Nunez P, Acuna-Aguilar LE, Gomez-Valles FO, Ramirez-Valdespino CA. Subtypes of Breast Cancer. In: Mayrovitz HN, editor. Breast Cancer. Brisbane (AU)2022.
6. Fragomeni SM, Sciallis A, Jeruss JS. Molecular Subtypes and Local-Regional Control of Breast Cancer. Surg Oncol Clin N Am. 2018;27(1):95-120.
7. Li Z, Wei H, Li S, Wu P, Mao X. The Role of Progesterone Receptors in Breast Cancer. Drug Des Devel Ther. 2022;16:305-14.
8. Waks AG, Winer EP. Breast Cancer Treatment: A Review. JAMA. 2019;321(3):288-300.
9. Hammond ME, Hayes DF, Dowsett M, Allred DC, Hagerty KL, Badve S, et al. American Society of Clinical Oncology/College Of American Pathologists guideline recommendations for immunohistochemical testing of estrogen and progesterone receptors in breast cancer. J Clin Oncol. 2010;28(16):2784-95.
10. Patel A, Unni N, Peng Y. The Changing Paradigm for the Treatment of HER2-Positive Breast Cancer. Cancers (Basel). 2020;12(8).
11. Bianchini G, Balko JM, Mayer IA, Sanders ME, Gianni L. Triple-negative breast cancer: challenges and opportunities of a heterogeneous disease. Nat Rev Clin Oncol. 2016;13(11):674-90.
12. Schmid P, Adams S, Rugo HS, Schneeweiss A, Barrios CH, Iwata H, et al. Atezolizumab and Nab-Paclitaxel in Advanced Triple-Negative Breast Cancer. N Engl J Med. 2018;379(22):2108-21.
13. Schmid P, Cortes J, Dent R, Pusztai L, McArthur H, Kummel S, et al. Event-free Survival with Pembrolizumab in Early Triple-Negative Breast Cancer. N Engl J Med. 2022;386(6):556-67.
14. Robson M, Im SA, Senkus E, Xu B, Domchek SM, Masuda N, et al. Olaparib for Metastatic Breast Cancer in Patients with a Germline BRCA Mutation. N Engl J Med. 2017;377(6):523-33.
15. Kazama T, Takahara T, Hashimoto J. Breast Cancer Subtypes and Quantitative Magnetic Resonance Imaging: A Systemic Review. Life (Basel). 2022;12(4).
16. Hsiao YH, Chou MC, Fowler C, Mason JT, Man YG. Breast cancer heterogeneity: mechanisms, proofs, and implications. J Cancer. 2010;1:6-13.
17. Lukasiewicz S, Czeczelewski M, Forma A, Baj J, Sitarz R, Stanislawek A. Breast Cancer-Epidemiology, Risk Factors, Classification, Prognostic Markers, and Current Treatment Strategies-An Updated Review. Cancers (Basel). 2021;13(17).
18. Gatti-Mays ME, Balko JM, Gameiro SR, Bear HD, Prabhakaran S, Fukui J, et al. If we build it they will come: targeting the immune response to breast cancer. NPJ Breast Cancer. 2019;5:37.
19. Ellulu MS, Patimah I, Khaza'ai H, Rahmat A, Abed Y. Obesity and inflammation: the linking mechanism and the complications. Arch Med Sci. 2017;13(4):851-63.
20. Quail DF, Dannenberg AJ. The obese adipose tissue microenvironment in cancer development and progression. Nat Rev Endocrinol. 2019;15(3):139-54.
21. Wang QL, Song M, Clinton SK, Mucci LA, Lagergren J, Giovannucci EL. Longitudinal trajectories of lifetime body shape and prostate cancer angiogenesis. Eur J Epidemiol. 2022;37(3):261-70.
22. Kolb R, Phan L, Borcherding N, Liu Y, Yuan F, Janowski AM, et al. Obesity-associated NLRC4 inflammasome activation drives breast cancer progression. Nat Commun. 2016;7:13007.
23. Onkar S, Cui J, Zou J, Cardello C, Cillo AR, Uddin MR, et al. Immune landscape in invasive ductal and lobular breast cancer reveals a divergent macrophage-driven microenvironment. Nat Cancer. 2023;4(4):516-34.
24. Riffelmacher T, Richter FC, Simon AK. Autophagy dictates metabolism and differentiation of inflammatory immune cells. Autophagy. 2018;14(2):199-206.
25. Madrigal-Matute J, de Bruijn J, van Kuijk K, Riascos-Bernal DF, Diaz A, Tasset I, et al. Protective role of chaperone-mediated autophagy against atherosclerosis. Proc Natl Acad Sci U S A. 2022;119(14):e2121133119.
26. Madrigal-Matute J, Cuervo AM. Regulation of Liver Metabolism by Autophagy. Gastroenterology. 2016;150(2):328-39.

27. Arias E, Cuervo AM. Pros and Cons of Chaperone-Mediated Autophagy in Cancer Biology. Trends Endocrinol Metab. 2020;31(1):53-66.
28. Mizushima N, Komatsu M. Autophagy: renovation of cells and tissues. Cell. 2011;147(4):728-41.
29. Florey O, Overholtzer M. Autophagy proteins in macroendocytic engulfment. Trends Cell Biol. 2012;22(7):374-80.
30. Behrooz AB, Cordani M, Fiore A, Donadelli M, Gordon JW, Klionsky DJ, et al. The obesity-autophagy-cancer axis: Mechanistic insights and therapeutic perspectives. Semin Cancer Biol. 2024;99:24-44.
31. Martinez-Lopez N, Tarabra E, Toledo M, Garcia-Macia M, Sahu S, Coletto L, et al. System-wide Benefits of Intermeal Fasting by Autophagy. Cell Metab. 2017;26(6):856-71 e5.
32. Nencioni A, Caffa I, Cortellino S, Longo VD. Fasting and cancer: molecular mechanisms and clinical application. Nat Rev Cancer. 2018;18(11):707-19.
33. Deleyto-Seldas N, Efeyan A. The mTOR-Autophagy Axis and the Control of Metabolism. Front Cell Dev Biol. 2021;9:655731.
34. Tasset I, Cuervo AM. Role of chaperone-mediated autophagy in metabolism. FEBS J. 2016;283(13):2403-13.
35. Kaushik S, Cuervo AM. Chaperone-mediated autophagy: a unique way to enter the lysosome world. Trends Cell Biol. 2012;22(8):407-17.
36. Gomes LC, Di Benedetto G, Scorrano L. During autophagy mitochondria elongate, are spared from degradation and sustain cell viability. Nat Cell Biol. 2011;13(5):589-98.
37. Hanahan D. Hallmarks of Cancer: New Dimensions. Cancer Discov. 2022;12(1):31-46.
38. Brandhorst S. Fasting and fasting-mimicking diets for chemotherapy augmentation. Geroscience. 2021;43(3):1201-16.
39. Kaushik S, Cuervo AM. The coming of age of chaperone-mediated autophagy. Nat Rev Mol Cell Biol. 2018;19(6):365-81.
40. Longo VD, Mattson MP. Fasting: molecular mechanisms and clinical applications. Cell Metab. 2014;19(2):181-92.
41. Lee AV, Oesterreich S, Davidson NE. MCF-7 cells--changing the course of breast cancer research and care for 45 years. J Natl Cancer Inst. 2015;107(7).
42. Mizushima N, Yoshimori T, Levine B. Methods in mammalian autophagy research. Cell. 2010;140(3):313-26.
43. Klionsky DJ, Abdel-Aziz AK, Abdelfatah S, Abdellatif M, Abdoli A, Abel S, et al. Guidelines for the use and interpretation of assays for monitoring autophagy (4th edition)(1). Autophagy. 2021;17(1):1-382.
44. Juste YR, Cuervo AM. Analysis of Chaperone-Mediated Autophagy. Methods Mol Biol. 2019;1880:703-27.
45. Lu TS, Yiao SY, Lim K, Jensen RV, Hsiao LL. Interpretation of biological and mechanical variations between the Lowry versus Bradford method for protein quantification. N Am J Med Sci. 2010;2(7):325-8.
46. Levine B, Klionsky DJ. Autophagy wins the 2016 Nobel Prize in Physiology or Medicine: Breakthroughs in baker's yeast fuel advances in biomedical research. Proc Natl Acad Sci U S A. 2017;114(2):201-5.
47. Mizushima N, Yoshimori T. How to interpret LC3 immunoblotting. Autophagy. 2007;3(6):542-5.
48. Romero-Calvo I, Ocon B, Martinez-Moya P, Suarez MD, Zarzuelo A, Martinez-Augustin O, et al. Reversible Ponceau staining as a loading control alternative to actin in Western blots. Anal Biochem. 2010;401(2):318-20.
49. Cui L, Zhao LP, Ye JY, Yang L, Huang Y, Jiang XP, et al. The Lysosomal Membrane Protein Lamp2 Alleviates Lysosomal Cell Death by Promoting Autophagic Flux in Ischemic Cardiomyocytes. Front Cell Dev Biol. 2020;8:31.
50. Han Q, Deng Y, Chen S, Chen R, Yang M, Zhang Z, et al. Downregulation of ATG5-dependent macroautophagy by chaperone-mediated autophagy promotes breast cancer cell metastasis. Sci Rep. 2017;7(1):4759.
51. Pankiv S, Clausen TH, Lamark T, Brech A, Bruun JA, Outzen H, et al. p62/SQSTM1 binds directly to Atg8/LC3 to facilitate degradation of ubiquitinated protein aggregates by autophagy. J Biol Chem. 2007;282(33):24131-45.
52. Komatsu M, Kageyama S, Ichimura Y. p62/SQSTM1/A170: physiology and pathology. Pharmacol Res. 2012;66(6):457-62.
53. Sahani MH, Itakura E, Mizushima N. Expression of the autophagy substrate SQSTM1/p62 is restored during prolonged starvation depending on transcriptional upregulation and autophagy-derived amino acids. Autophagy. 2014;10(3):431-41.

54. Bjorkoy G, Lamark T, Pankiv S, Overvatn A, Brech A, Johansen T. Monitoring autophagic degradation of p62/SQSTM1. Methods Enzymol. 2009;452:181-97.
55. Liu WJ, Ye L, Huang WF, Guo LJ, Xu ZG, Wu HL, et al. p62 links the autophagy pathway and the ubiqutin-proteasome system upon ubiquitinated protein degradation. Cell Mol Biol Lett. 2016;21:29.
56. Mitchell SJ, Madrigal-Matute J, Scheibye-Knudsen M, Fang E, Aon M, Gonzalez-Reyes JA, et al. Effects of Sex, Strain, and Energy Intake on Hallmarks of Aging in Mice. Cell Metab. 2016;23(6):1093-112.
57. Vargas JNS, Hamasaki M, Kawabata T, Youle RJ, Yoshimori T. The mechanisms and roles of selective autophagy in mammals. Nat Rev Mol Cell Biol. 2023;24(3):167-85.

8. Annexes

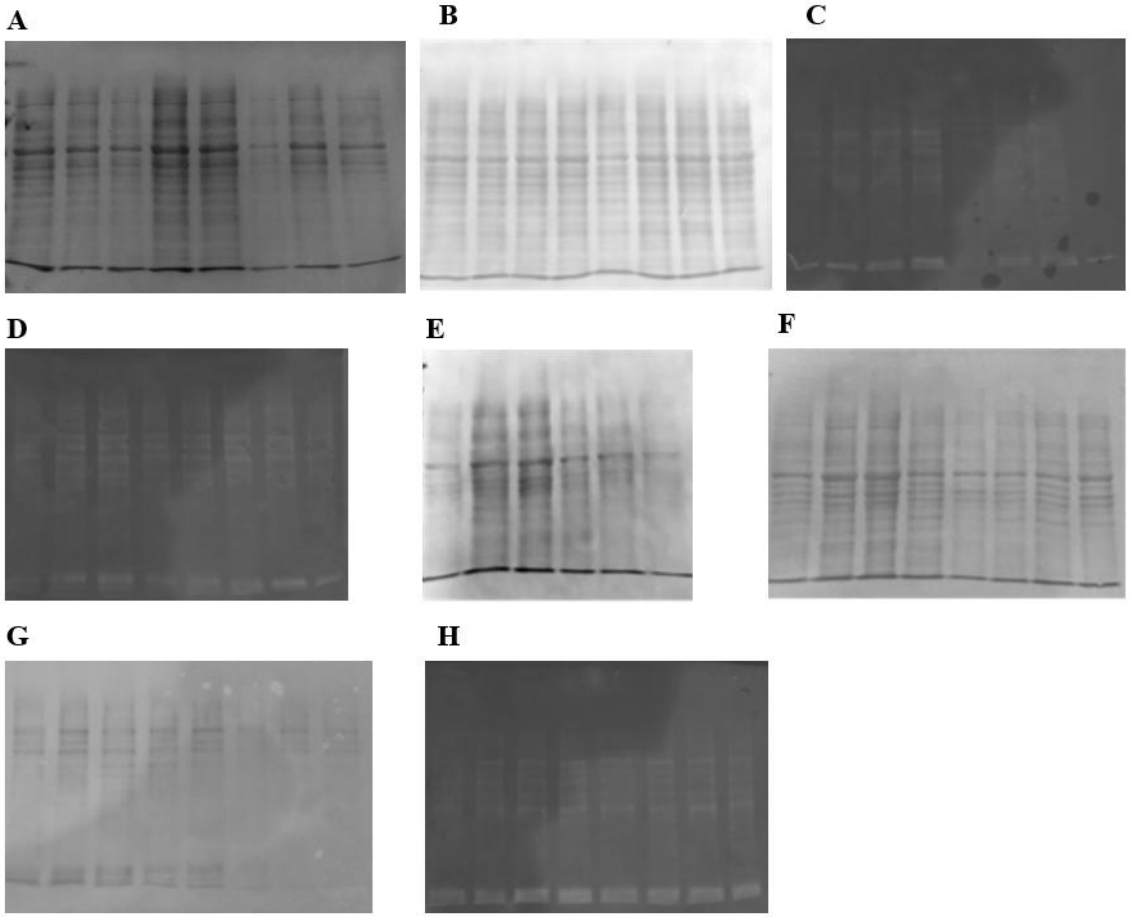

Figure A1. *Ponceau S staining of Western blot membranes used in the analysis of macroautophagy (MA) and chaperone-mediated autophagy (CMA) under different intermittent fasting cycles in MCF-7 cells. The following conditions were loaded from left to right in each membrane: Ct, Ct+i, A1, A1+i, A2, A2+i, A3, A3+i.* ***(A)*** *MA, 12% gel, n=1;* ***(B)*** *MA, 12% gel, n=2;* ***(C)*** *MA, 15% gel, n=1;* ***(D)*** *MA, 15% gel, n=2;* ***(E)*** *CMA, 12% gel, n=1 (A3 and A3+i were lost);* ***(F)*** *CMA, 12% gel, n=2;* ***(G)*** *CMA, 15% gel, n=1;* ***(H)*** *CMA, 15% gel, n=2.*